Phase transitions in self-gravitating systems: Self-gravitating fermions and hard-sphere models

Pierre-Henri Chavanis
Laboratoire de Physique Quantique, Université Paul Sabatier, 118 route de Narbonne, 31062 Toulouse, France
(Received 18 September 2001; revised manuscript received 31 January 2002; published 20 May 2002)

We discuss the nature of phase transitions in self-gravitating systems both in the microcanonical and in the canonical ensemble. We avoid the divergence of the gravitational potential at short distances by considering the case of self-gravitating fermions and hard-sphere models. Depending on the values of the parameters, three kinds of phase transitions (of zeroth, first, and second order) are evidenced. They separate a ''gaseous'' phase with a smoothly varying distribution of matter from a ''condensed'' phase with a core-halo structure. We propose a simple analytical model to describe these phase transitions. We determine the value of energy (in the microcanonical ensemble) and temperature (in the canonical ensemble) at the transition point and we study their dependance on the degeneracy parameter (for fermions) or on the size of the particles (for a hard-sphere gas). Scaling laws are obtained analytically in the asymptotic limit of a small short distance cutoff. Our analytical model captures the essential physics of the problem and compares remarkably well with the full numerical solutions. We also stress some analogies with the liquid-gas transition and with the Blume-Emery-Griffiths model with infinite range interactions. In particular, our system presents two tricritical points at which the transition passes from first order to second order.

DOI: 10.1103/PhysRevE.65.056123 PACS number(s): 05.90.+m, 64.60.−i, 47.20.−k, 05.70.−a

I. INTRODUCTION

The statistical mechanics of self-gravitating systems turns out to be very different from that of other, more familiar, many-body systems, e.g., neutral gases and plasmas, due to the unshielded, long-range nature of the gravitational force [1]. Due to this fundamental difference, the notion of equilibrium is not always well defined and these systems exhibit a nontrivial behavior with the occurence of phase transitions associated with gravitational collapse. If the particles are treated as classical point masses, it can be shown that no global entropy maximum exists, even if the system is restricted within a box so as to prevent evaporation [2,3]. A self-gravitating system can increase entropy without bound by developing a dense and hot ''core'' surrounded by a dilute ''halo.'' There exist, however, local entropy maxima (metastable equilibrium states) if the condition $\Lambda=-ER/GM^2 \leqslant 0.335$ is satisfied, i.e., if the energy E is sufficiently large (for a given box radius R) or if the radius is sufficiently small (for a given energy E). Since these equilibrium states are only *local* entropy maxima, the question naturally emerges whether they are long-lived or will collapse to a configuration with higher entropy. In any case, a phase transition *must* occur for $\Lambda>\Lambda_c=0.335$ since the entropy has no extremum at all above this threshold [2]. In that case, the system is expected to collapse indefinitely towards a state of higher and higher central concentration and temperature. This is the celebrated ''gravothermal catastrophe'' [3].

However, if we introduce a repulsive potential at short distances, complete core collapse is prevented and it can be proved that a global entropy maximum now exists for all accessible values of energy. This effective repulsion can be introduced in many different ways but the physical results are rather insensitive to the precise form of the regularization. For example, we can study the case of self-gravitating fermions for which an exclusion principle imposes an upper bound on the distribution function [4–7]. Alternatively, we can consider a classical hard-sphere gas by introducing an ''excluded volume'' around each particle [8,9]. Other forms of regularization are possible [10,11]. When such regularizations are introduced, it is possible to evidence properly three kinds of phase transitions of zeroth, first, and second order. They separate a ''gaseous'' phase, which is independant of the small-scale cutoff, from a ''condensed'' phase in which the particles are tightly bound. This is similar to the liquid-gas transition in an ordinary fluid. However, for long-range systems, such as self-gravitating systems, the statistical ensembles are not interchangeable and phase transitions can occur both in the canonical and in the microcanonical ensemble. This results in the existence of *two* tricritical points, one in each ensemble. In that respect the self-gravitating Fermi gas shares some analogies with the Blume-Emery-Griffiths (BEG) model with infinite range interactions [12].

The object of this paper is to provide a detailed description of phase transitions in self-gravitating systems. In Secs. II–V we consider the case of self-gravitating fermions. The equilibrium phase diagram was calculated in an earlier paper [6] and we complete this study by determining explicitly the values of energy (in the microcanonical ensemble) and temperature (in the canonical ensemble) at which the phase transitions occur. We also propose a simple analytical model to describe these phase transitions. The ''gaseous'' phase is modeled by a classical homogeneous sphere while the ''condensed'' phase is made of a completely degenerate nucleus surrounded by a hot atmosphere with uniform density (restrained by the box). The mass M_* of the nucleus is determined by maximizing the entropy (free energy) vs M_* for a given total mass and energy (temperature) of the configuration. Quite remarkably, this simple model can reproduce the main features of the numerical study. It also allows us to determine analytically how the energy or the temperature at the transition points depend on the degeneracy parameter. In Sec. VI we extend our analytical model to the case of a classical gas with a short distance cutoff. This model has

been studied numerically by Aronson and Hansen [8] and Stahl *et al.* [9], and our analytical model gives a good agreement with their numerical results. It is also consistent with the toy models of Lynden-Bell and Lynden-Bell [13] and Padmanabhan [1]. The possible astrophysical applications of our study are discussed in Sec. VI E.

II. STATISTICAL MECHANICS OF SELF-GRAVITATING FERMIONS

A. The Fermi-Dirac distribution

We consider a system of N fermions interacting via Newtonian gravity. These particles can be electrons in white dwarf stars [14], neutrons in neutron stars [15,4], massive neutrinos in dark matter models [16,5], etc. We assume that the mass of the configuration is sufficiently small so as to ignore general relativistic effects. Let $f(\mathbf{r},\mathbf{v},t)$ denote the distribution function of the system, i.e., $f(\mathbf{r},\mathbf{v},t)d^3\mathbf{r}d^3\mathbf{v}$ gives the mass of particles whose positions and velocities are in the cell $(\mathbf{r},\mathbf{v};\mathbf{r}+d^3\mathbf{r},\mathbf{v}+d^3\mathbf{v})$ at time t. The integral of f over the velocity determines the spatial density

$$\rho=\int f d^3\mathbf{v}, \tag{1}$$

and the total mass of the configuration is given by

$$M=\int \rho d^3\mathbf{r}, \tag{2}$$

where the integral extends over the entire domain. On the other hand, in the mean-field approximation, the total energy of the system can be expressed as

$$E=\frac{1}{2}\int f v^2 d^3\mathbf{r}d^3\mathbf{v}+\frac{1}{2}\int \rho\Phi d^3\mathbf{r}=K+W, \tag{3}$$

where K is the kinetic energy and W is the potential energy. The gravitational potential Φ is related to the star density by the Newton-Poisson equation

$$\Delta\Phi=4\pi G\rho. \tag{4}$$

Finally, the Fermi-Dirac entropy is given by the formula

$$S=-\int\left\{\frac{f}{\eta_0}\ln\frac{f}{\eta_0}+\left(1-\frac{f}{\eta_0}\right)\ln\left(1-\frac{f}{\eta_0}\right)\right\}d^3\mathbf{r}d^3\mathbf{v}, \tag{5}$$

which can be obtained by a standard combinatorial analysis. In this expression, η_0 is the maximum value accessible to the distribution function. If $g=2s+1$ denotes the spin multiplicity of the quantum states, m the mass of the particles, and h the Planck constant, one has by virtue of the Pauli exclusion principle $\eta_0=gm^4/h^3$. An entropy of the form (5) was also introduced by Lynden-Bell [17] in the context of collisionless self-gravitating systems (e.g., elliptical galaxies, dark matter) undergoing a ''violent relaxation'' by phase mixing [18–20]. In that context, η_0 represents the maximum value of the initial distribution function and the actual distribution function (coarse-grained) must always satisfy $\overline{f}\leqslant\eta_0$ by virtue of the Liouville theorem. This is the origin of the ''effective'' exclusion principle in Lynden-Bell's theory, which has nothing to do with quantum mechanics. In reality, the mixing entropy introduced by Lynden-Bell is a complicated sum of Fermi-Dirac entropies for each phase level constituting the initial condition. For simplicity, we shall restrict ourselves to the single level approximation for which the mixing entropy coincides with expression (5).

At statistical equilibrium, the system is expected to maximize the Fermi-Dirac entropy at fixed mass and energy. Introducing Lagrange multipliers to satisfy these constraints, we find that the *critical points* of entropy correspond to the Fermi-Dirac distribution

$$f=\frac{\eta_0}{1+\lambda e^{\beta((v^2/2)+\Phi)}}, \tag{6}$$

where λ is a strictly positive constant, ensuring that $f\leqslant\eta_0$ and β is the inverse temperature. In the fully degenerate limit $f\simeq\eta_0$, this distribution function has been extensively studied in the context of white dwarf stars in which gravity is balanced by the pressure of a degenerate electron gas [14]. In the nondegenerate limit $f\ll\eta_0$, the Fermi-Dirac distribution reduces to the Maxwell-Boltzmann distribution

$$f\simeq\frac{\eta_0}{\lambda}e^{-\beta((v^2/2)+\Phi)}, \tag{7}$$

so that we expect to recover the properties of classical isothermal spheres at low densities [1]. In particular, the Fermi-Dirac spheres, like the isothermal spheres, have an infinite mass and one is forced to confine the system within a box of radius R. Physically, this confinement is justified by the realization that the relaxation is *incomplete* so that the conditions of applicability of statistical mechanics, regarding, for example, the ergodic hypothesis, can be fulfilled only in a limited region of space. In addition, an astrophysical system is never completely isolated and R could represent the typical radius at which the system interacts with its neighbors.

Kinetic equations have been proposed to describe the relaxation of self-gravitating systems towards the Fermi-Dirac distribution [18,21]. If we assume that the system is subject to tidal forces and if we allow high energy particles to escape the system when they reach an energy $\epsilon=v^2/2+\Phi\geqslant\epsilon_m$, an extension of the Michie-King model taking into account the degeneracy can be deduced from these equations [21]. For $\epsilon\leqslant\epsilon_m$, one has

$$f=\eta_0\frac{e^{-\beta\epsilon}-e^{-\beta\epsilon_m}}{\lambda+e^{-\beta\epsilon}}, \tag{8}$$

while $f=0$ for $\epsilon>\epsilon_m$ since the stars have been removed by the tidal field. When $\lambda\to+\infty$, we recover the Michie-King model [22] and when $\epsilon_m\to+\infty$, we recover the Fermi-Dirac distribution (6). The density associated with the truncated distribution function (8) goes to zero at a finite radius, which is identified as the tidal radius. Therefore, the configuration

has a finite mass. This distribution function could describe elliptical galaxies and galactic halos limited in extension as a consequence of tidal interactions with other systems [17,16]. This model is, of course, more realistic than the box model. However, in order to exhibit phase transitions in self-gravitating systems, the box model provides a more convenient theoretical framework and we shall use it in the sequel.

B. Thermodynamical parameters

The thermodynamical parameters for Fermi-Dirac spheres in the mean-field approximation have been calculated by Chavanis and Sommeria [6] and we shall directly use their results. The equation determining the gravitational potential at equilibrium is obtained by substituting the Fermi-Dirac distribution (6) in the Poisson Eq. (4), using Eq. (1). Introducing the variables $\psi=\beta(\Phi-\Phi_0)$, where Φ_0 is the central potential, $k=\lambda e^{\beta\Phi_0}$, and $\xi=(16\pi^2\sqrt{2}G\eta_0/\beta^{1/2})^{1/2}r$, it can be written

$$\frac{1}{\xi^2}\frac{d}{d\xi}\left(\xi^2\frac{d\psi}{d\xi}\right)=I_{1/2}(ke^{\psi(\xi)}), \tag{9}$$

where $I_{1/2}$ denotes the Fermi integral

$$I_n(t)=\int_0^{+\infty}\frac{x^n}{1+te^x}dx \tag{10}$$

of order $n=1/2$. The boundary conditions at the origin are

$$\psi(0)=\psi'(0)=0. \tag{11}$$

In the case of bounded spheres, one must stop the integration of Eq. (9) at $\xi=\alpha$ with

$$\alpha=\left(\frac{16\pi^2\sqrt{2}G\eta_0}{\beta^{1/2}}\right)^{1/2}R. \tag{12}$$

The parameter α is related to the temperature and to the energy by the equations

$$\eta\equiv\frac{\beta GM}{R}=\alpha\psi_k'(\alpha), \tag{13}$$

$$\Lambda\equiv-\frac{ER}{GM^2}=\frac{\alpha^7}{\mu^4}\int_0^{\alpha}I_{3/2}(ke^{\psi_k(\xi)})\xi^2d\xi-\frac{2}{3}\frac{\alpha^{10}}{\mu^4}I_{3/2}(ke^{\psi_k(\alpha)}). \tag{14}$$

Moreover, α and k are related to each other by the relation

$$\alpha^5\psi_k'(\alpha)=\mu^2, \tag{15}$$

where μ is the "degeneracy parameter,"

$$\mu=\eta_0\sqrt{512\pi^4G^3MR^3}. \tag{16}$$

For a given value of μ and k, we can solve the ordinary differential equation (9) until the value $\xi=\alpha$ at which the condition (15) is satisfied. Then, Eqs. (13) and (14) determine the temperature and the energy of the configuration. By varying the parameter k (for a fixed value of the degeneracy parameter μ), we can cover the whole bifurcation diagram in parameter space [6]. The entropy of each configuration is given by (see the Appendix)

$$\frac{S\eta_0}{M}=-\frac{7}{3}\Lambda\eta+\psi_k(\alpha)+\eta+\ln k-\frac{2\alpha^6}{9\mu^2}I_{3/2}(ke^{\psi_k(\alpha)}), \tag{17}$$

and the free energy by

$$J=S-\beta E. \tag{18}$$

Note that Eq. (18) is the free energy $F=E-TS$ up to a negative proportionality factor. In the microcanonical ensemble, a solution is stable if it corresponds to a maximum of entropy S at fixed mass and energy. In the canonical ensemble, the condition of stability requires that the solution be a maximum of free energy J at fixed mass and temperature. It can be shown [4] that this mean-field approach is *exact* in a thermodynamical limit such that $N\to+\infty$ with μ, η, Λ fixed. This implies, in particular, that $N^{1/3}R$, $TN^{-4/3}$, $EN^{-7/3}$, and SN^{-1} approach a constant value for $N\to+\infty$. The usual thermodynamical limit $N,R\to+\infty$ with N/R^3 constant is, of course, not relevant for nonextensive systems.

III. PHASE TRANSITIONS IN A SELF-GRAVITATING FERMI GAS

A. The nondegenerate limit ($\mu=\infty$)

Before considering the case of an arbitrary degree of degeneracy, it may be useful to discuss first the nondegenerate limit corresponding to a classical isothermal gas ($\hbar\to0$). In that case, the thermodynamical parameters are given by [3]

$$\eta=\alpha\psi'(\alpha), \tag{19}$$

$$\Lambda=\frac{3}{2}\frac{1}{\alpha\psi'(\alpha)}-\frac{e^{-\psi(\alpha)}}{\psi'(\alpha)^2}, \tag{20}$$

$$\frac{S}{N}=-\frac{1}{2}\ln\eta-2\ln\alpha+\psi(\alpha)+\eta-2\Lambda\eta, \tag{21}$$

where $\alpha=(4\pi G\beta\rho_0)^{1/2}R$ is the normalized box radius and ψ is the normalized gravitational potential solution of the Emden equation [14]

$$\frac{1}{\xi^2}\frac{d}{d\xi}\left(\xi^2\frac{d\psi}{d\xi}\right)=e^{-\psi} \tag{22}$$

with boundary conditions

$$\psi(0)=\psi'(0)=0. \tag{23}$$

The equilibrium phase diagram (E,T) is represented in Fig. 1. The curve is parametrized by α, which can be considered as a measure of the central concentration. An equivalent parametrization is provided by the density contrast $\mathcal{R}=\rho(0)/\rho(R)$ (see Fig. 2). In the microcanonical ensemble

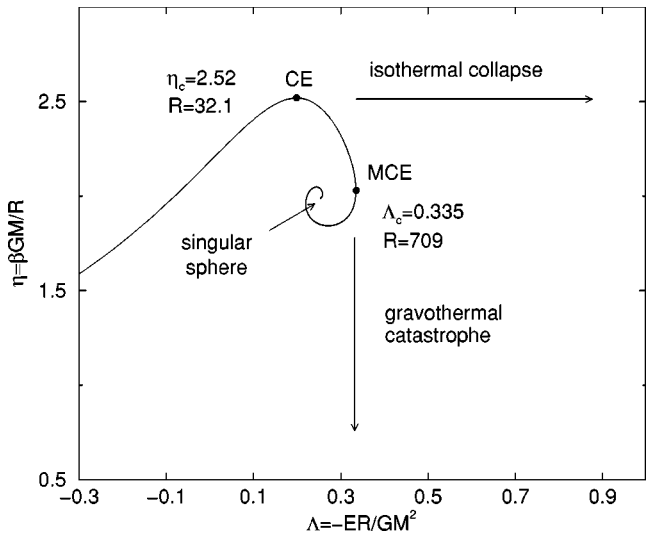

FIG. 1. Equilibrium phase diagram for classical isothermal spheres. For $\Lambda > \Lambda_c$ or $\eta > \eta_c$, there is no hydrostatic equilibrium and the system undergoes a gravitational collapse.

(MCE), the solutions on the upper branch of Fig. 1 (until point MCE) are stable and correspond to local entropy maxima. The rest of the spiral corresponds to unstable saddle points. For $\Lambda > \Lambda_c = 0.335$, there are no critical points of entropy and the system collapses indefinitely. This is the so-called ''gravothermal catastrophe.'' In the canonical ensemble (CE), only the solutions prior to point CE are stable. They correspond to local maxima of free energy. The rest of the spiral corresponds to unstable saddle points. For $\eta > \eta_c = 2.52$, there is no hydrostatic equilibrium and the system undergoes an ''isothermal collapse.'' These stability results can be deduced from the turning point analysis of Katz [23] or by solving the eigenvalue equations associated with the

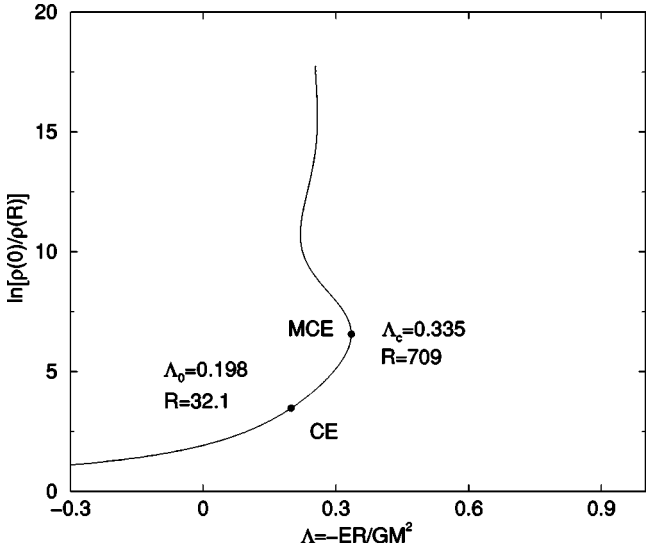

FIG. 2. Density contrast of classical isothermal spheres as a function of energy. The series of equilibria becomes unstable in the canonical ensemble for $\mathcal{R} > 32.1$ and in the microcanonical ensemble for $\mathcal{R} > 709$. The value of energy at which the density contrast tends to $+\infty$ is $\Lambda = 1/4$ (singular sphere).

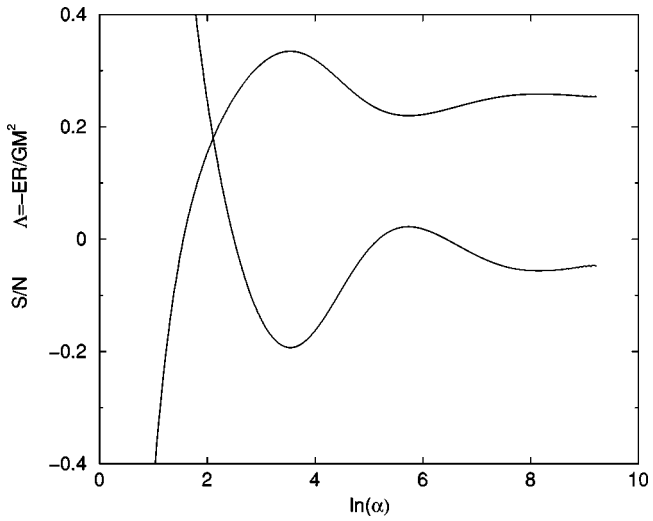

FIG. 3. Entropy and energy as functions of the central concentration α. The peaks of energy and entropy occur for the same values of α.

second order variations of entropy or free energy [24,25]. For $\Lambda < \Lambda_c$ and $\eta < \eta_c$, the stable solutions are only *metastable*. There are no global maxima of entropy or free energy for classical point masses in gravitational interaction [2]. We also note that the region of negative specific heats (between points CE and MCE) is stable in the microcanonical ensemble and unstable in the canonical ensemble, where it is replaced by a phase transition (an ''isothermal collapse''). This is expected on physical grounds since it can be shown quite generally that the specific heat *must* be positive in the canonical ensemble [1]. These results clearly indicate that the statistical ensembles are not interchangeable in the case of self-gravitating systems (see, e.g., Ref. [26]), contrary to normal matter in which the energy is an extensive parameter.

In Fig. 3, we have plotted the energy and entropy as func-

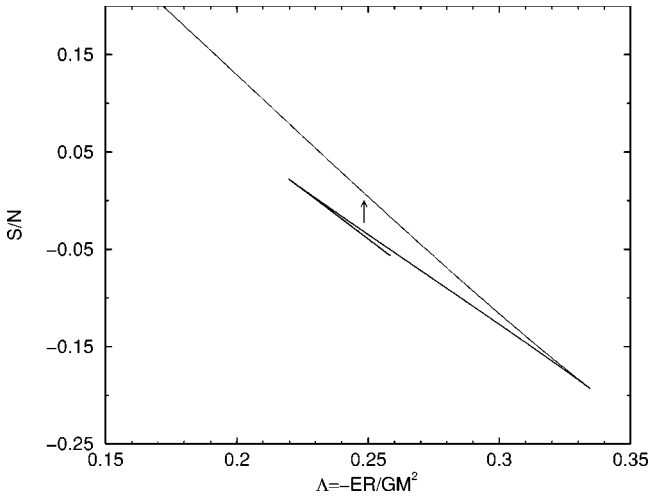

FIG. 4. Entropy vs energy for classical isothermal spheres. When several solutions exist for the same energy, the states with low entropy are unstable saddle points. They can either evolve towards the metastable state with highest entropy (see arrow) or collapse to a state of ever-increasing entropy, as suggested in Ref. [26].

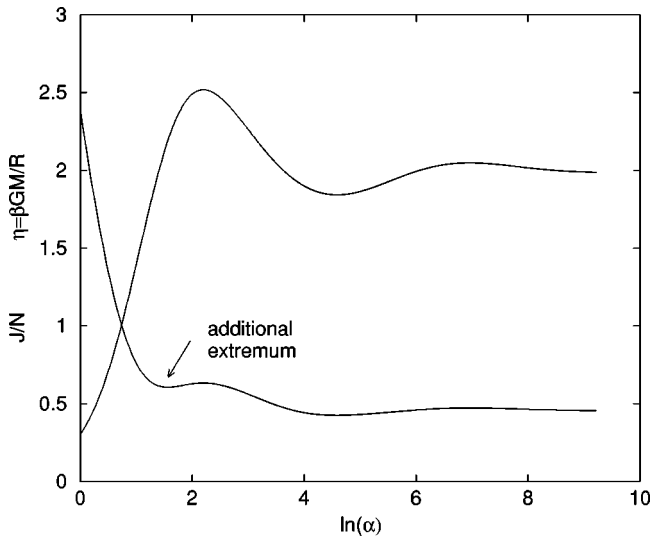

FIG. 5. Free energy and inverse temperature as functions of the central concentration α. The peaks occur for the same values of α. The free energy presents an additional extremum, but it is not associated with an instability.

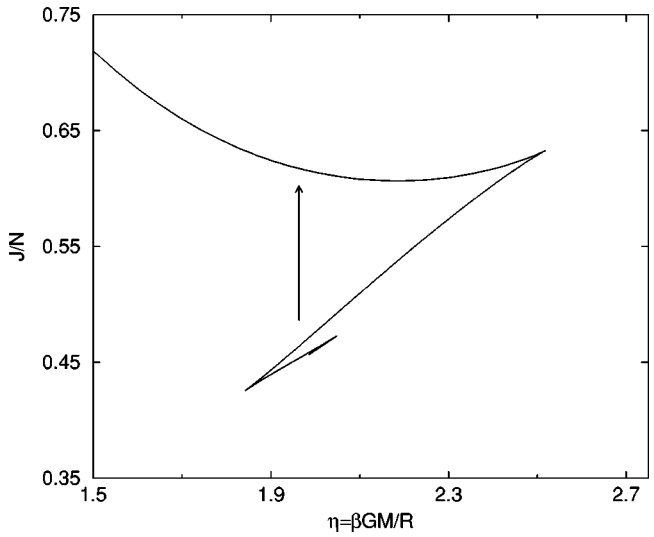

FIG. 6. Free energy vs inverse temperature for classical isothermal spheres. The interpretation is the same as in Fig. 4.

tions of the central concentration α. We observe that the peaks occur for the same values of α, since $dS=\beta dE$. This is also clear from Fig. 4 where we have represented the entropy as a function of energy. When several critical points of entropy exist for the same energy, only the one with the largest entropy is an entropy *maximum*. The other critical points are unstable saddle points. Therefore, if the system is initially prepared on a saddle point, we expect a transition to occur from a state of low entropy to a state of higher entropy. This is not really a phase transition but just an instability. A similar diagram has been found for isothermal spheres described in the context of general relativity [27]. In this analogy, the mass energy M plays the role of the classical energy E and the binding energy $E_{bind}=(M-M_0)c^2$, where $M_0=Nm$ is the rest mass and N the baryon number, plays the role of the classical entropy S. In Figs. 5 and 6, we have ploted the corresponding diagrams in the canonical ensemble. Here again, the peaks of temperature correspond to the peaks of free energy, since $dS=-Ed\beta$. The free energy has an additional peak (for $E=0$), which has no counterpart in the temperature diagram. However, this peak is not associated with an instability and the interpretation of the curves is the same as in the microcanonical ensemble.

B. Large values of the degeneracy parameter ($\mu=10^5$)

We now consider the case of self-gravitating fermions characterized by a degeneracy parameter μ. We first discuss the case of large values of the degeneracy parameter. The extension of the classical diagram of Fig. 1 is reported in Fig. 7. We see that the inclusion of degeneracy has the effect of unwinding the spiral. The evolution of the density contrast along the series of equilibrium is depicted in Fig. 8. In the range $\Lambda_*(\mu)<\Lambda<\Lambda_c$, there exist several critical points of entropy for each single value of energy. The solutions on the upper branch of Fig. 7 (points A) are nondegenerate and have a smooth density profile; they form the ''gaseous'' phase. The solutions on the lower branch (points C) have a ''core-halo'' structure with a massive degenerate nucleus and a dilute atmosphere; they form the ''condensed'' phase. According to the criterion of Katz [23], specifically discussed in Ref. [6] for self-gravitating fermions, these solutions are both entropy maxima (EM), while the intermediate solutions (points B) are unstable saddle points (SP). These points are similar to points A, except that they contain a small embryonic nucleus (with small mass and energy) which plays the role of a ''germ'' in the langage of phase transition. The density profiles of these solutions are given in Ref. [6].

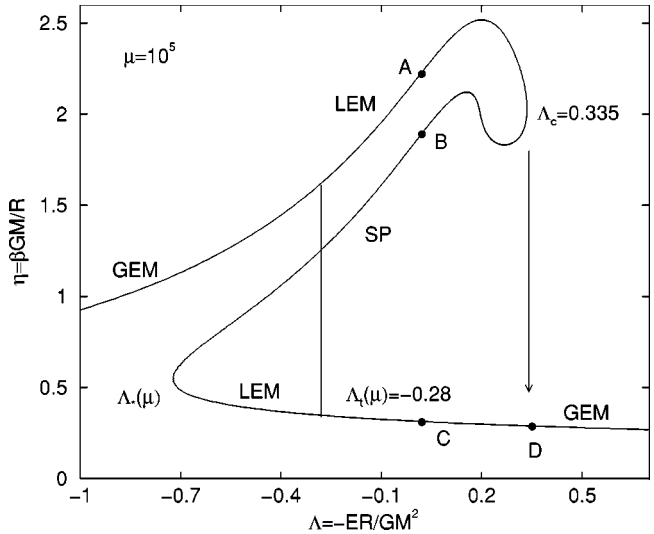

FIG. 7. Equilibrium phase diagram for Fermi-Dirac spheres with a degeneracy parameter $\mu=10^5$. Points A form the ''gaseous'' phase. They are global entropy maxima (GEM) for $\Lambda<\Lambda_t(\mu)$ and local entropy maxima (LEM) for $\Lambda>\Lambda_t(\mu)$. Points C form the ''condensed'' phase. They are LEM for $\Lambda<\Lambda_t(\mu)$ and GEM for $\Lambda>\Lambda_t(\mu)$. Points B are unstable SP and contain a ''germ.'' This figure exhibits, in particular, a first order phase transition in the microcanonical ensemble.

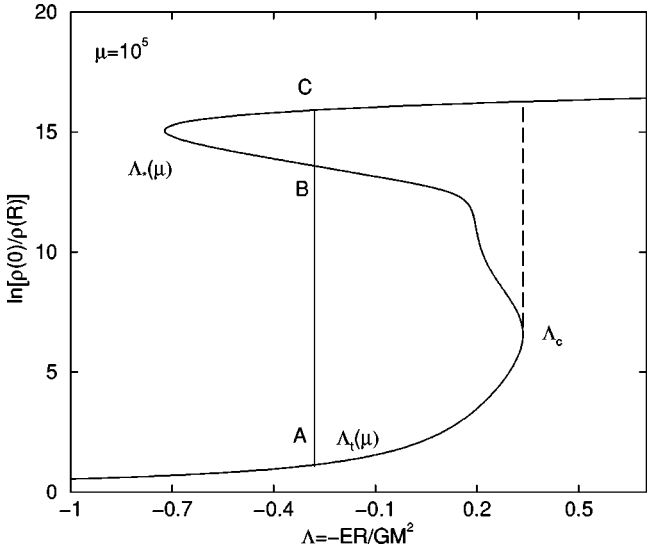

FIG. 8. Density contrast as a function of energy for self-gravitating fermions ($\mu=10^5$). This figure can be compared with Fig. 2 for classical isothermal spheres. Points *A* (gaseous phase) have a low density contrast. Points *B* and *C* contain a central nucleus with high density [6].

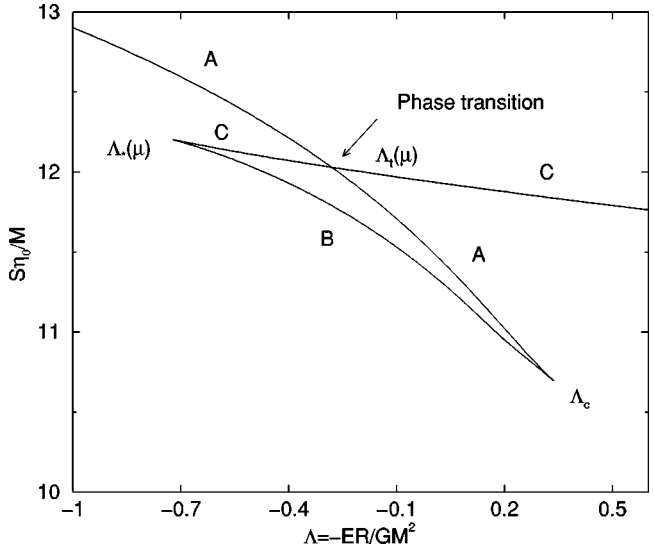

FIG. 9. Entropy of each phase vs energy for $\mu=10^5$. A phase transition occurs at $\Lambda_t(\mu)$ at which the two stable branches (solutions *A* and *C*) intersect. The unstable solutions *B* always have smaller entropy.

To be more precise, we have plotted the entropy of these solutions as a function of energy in Fig. 9. The entropy of the unstable phase (points *B*) is always smaller than the entropy of the stable phases, as it should. There is now a crossing point in the diagram, at $\Lambda=\Lambda_t(\mu)$, which marks the onset of a phase transition. At that point, the ''gaseous'' phase and the ''condensed'' phase have the same entropy. As Λ is increased across the transition point, the nondegenerate solutions (points *A*) pass from global to local entropy maxima. Inversely, the degenerate solutions (points *C*) pass from local to global entropy maxima. We expect, therefore, a phase transition to occur from the ''gaseous'' phase to the ''condensed'' phase when $\Lambda=\Lambda_t^+(\mu)$. The ''kink'' in the curve $S(E)$ at the transition point where the two branches intersect corresponds to a discontinuity of temperature in the equilibrium phase diagram (see the vertical plateau in Fig. 7). The specific heat is also discontinuous at that point and turns from positive to negative. According to Stahl *et al.* [9], this phase transition could be called a ''gravitational first order phase transition.'' It has to be noted, however, that contrary to the liquid-vapor transition, the two phases cannot coexist in the present situation.

For $\Lambda_t(\mu)<\Lambda<\Lambda_c$, the nondegenerate solutions are metastable, but we may suspect [6] that they are long-lived so that they *are* physical. These solutions are insensitive to the small-scale regularization and depend only on the long-range gravitational interaction. In the limit $\mu\to+\infty$, the transition energy $\Lambda_t(\mu)$ goes to $-\infty$ and we recover the classical spiral of Fig. 1. This spiral is formed by the metastable states of the ''gaseous'' phase (points *A*). The ''condensed'' phase (points *C*) is superposed to the Λ axis. These states have an infinite central density and an infinite temperature. The unstable branch (points *B*) coincides with the spiral, but these states physically differ from the ''gaseous'' states (points *A*) by the presence of an infinitesimal ''germ'' with negligible mass and energy. Therefore, what we see actually in the limit $\mu\to+\infty$ are the metastable states. It is plausible that these metastable states will be selected by the dynamics (on relevant time scales) even if states with higher entropy exist. In fact, depending on its *topology* (i.e., the form of the profile) an initial condition with $\Lambda>\Lambda_t(\mu)$ can either relax towards the local entropy maximum (gaseous phase) or collapse towards the global entropy maximum (condensed phase). Alternatively, for $\Lambda<\Lambda_t(\mu)$ an initially ''condensed'' configuration can remain frozen in this metastable state or explode into a ''gaseous'' state with more entropy. Therefore, the choice of a stable equilibrium state does not only depend on whether the equilibrium solution is a local or a global entropy maximum, but also on whether or not the initial condition lies in its ''basin of attraction''. The characterization of this basin of attraction requires a nonequilibrium analysis, which is not attempted in the present paper. A first step in that direction was performed by Youngkins and Miller [11] by using a one-dimensional spherical shell model and by Chavanis *et al.* [26] with the aid of a simple relaxation equation derived from a maximum entropy production principle [18]. These preliminary works reveal that the structure of this basin of attraction is extremely complex so that the final state of the system cannot be easily predicted from the initial condition when several entropy maxima exist. In addition, the structure of this basin of attraction also depends on whether the system is described by the microcanonical or by the canonical ensemble [11,26].

However, for $\Lambda>\Lambda_c$ the metastable phase completely disappears and, in that case, the system *must* necessarily collapse. This transition is associated with what has been traditionally called the ''gravothermal catastrophe'' [3] in the case of classical point masses. For systems described by the Fermi-Dirac statistics, the core ultimately ceases to shrink when it becomes degenerate. In that case, the system falls on to the global entropy maximum (point *D*), which is the true

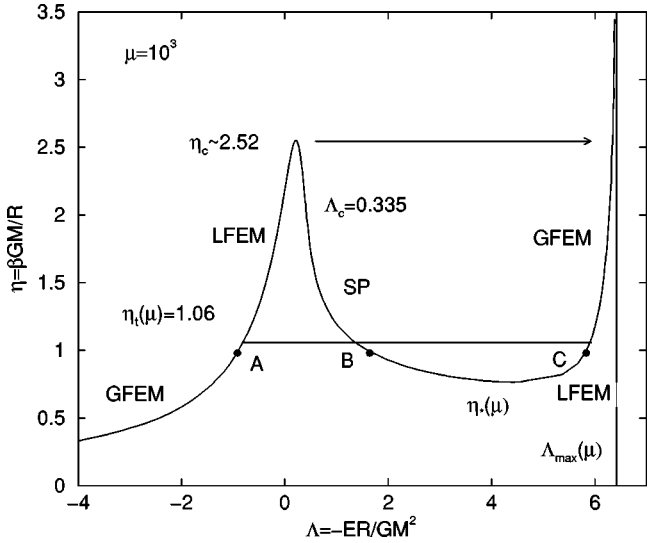

FIG. 10. Equilibrium phase diagram for Fermi-Dirac spheres with a degeneracy parameter $\mu=10^3$. Points *A* form the ''gaseous'' phase. They are global maxima of free energy (GFEM) for $\eta<\eta_t$ and local maxima of free energy (LFEM) for $\eta>\eta_t$. The reverse is true for points *C* in the ''condensed'' phase. Points *B* are unstable SP. This figure exhibits, in particular, a first order phase transition in the canonical ensemble. The equality of the free energy of the two phases ($J_A=J_C$) at the transition temperature η_t implies the equality of the areas delimited by the curve and the plateau, i.e., $\int_A^C(\eta-\eta_t)d\Lambda=0$. This is similar to Maxwell's construction in the theory of the van der Waals gas.

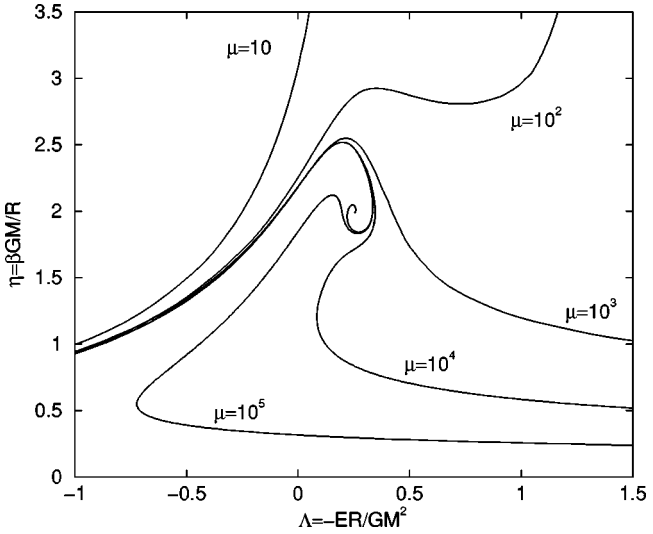

FIG. 11. Equilibrium phase diagram for self-gravitating fermions with different values of the degeneracy parameter μ. The zeroth and first order phase transitions are suppressed in the microcanonical ensemble for $\mu\lesssim 2600$ and in the canonical ensemble for $\mu\lesssim 82.5$. For large values of μ, the curve makes several rotations before unwinding. The criterion of Katz tells us that one mode of stability is lost each time the curve rotates clockwise and regained as the curve rotates counterclockwise. Therefore, only the upper and lower branches are entropy maxima. For $\mu\to+\infty$ (classical limit), the curve winds up indefinitely and tends to the spiral of Fig. 1 as discussed in the text.

equilibrium state for these systems. This global entropy maximum has a ''core-halo'' structure, with a degenerate core and a nondegenerate halo. This phase transition is sometimes called a zeroth order phase transition [28] since it is associated with a discontinuous jump of entropy (in the classical limit, the entropy of the condensed phase is infinite). In fact, this does not correspond to a true phase transition (in the usual sense), not even to an instability, but simply to the sudden disapearance of the ''gaseous'' phase. It has to be noted that the degenerate nucleus resulting from this gravitational collapse has a relatively important mass and a very small radius (for $\mu=10^5$ and $\Lambda\simeq\Lambda_c$, we have typically $M_*/M\simeq 0.22$ and $R_*/R\simeq 5\ \ 10^{-3}$). This massive nucleus (fermion ball) can have important astrophysical implications and, in the context of dark matter, may mimic the effect of a black hole at the center of a galaxy (see Sec. VI E).

C. Small values of the degeneracy parameter ($\mu=10^3$)

When the degeneracy parameter is sufficiently small, there exists only one critical point of entropy for each value of energy (see Fig. 10) and it is a global entropy maximum. Therefore, a sufficiently strong degeneracy suppresses the phase transitions in the microcanonical ensemble, including the ''gravothermal catastrophe'' (see Fig. 11). For high energies (small values of Λ) the solutions almost coincide with the classical isothermal spheres. When the energy is lowered (large values of Λ) the solutions take a ''core-halo'' structure with a partially degenerate nucleus surrounded by a dilute Maxwellian atmosphere. It is now possible to overcome the critical energy $\Lambda_c=0.335$ and the critical density contrast $\mathcal{R}=709$ found by Antonov [2] for classical particles. In that region, the specific heat is negative, which is allowed in the microcanonical ensemble. As energy decreases further, more and more mass is concentrated in the nucleus (which becomes more and more degenerate) until a minimum accessible energy, corresponding to $\Lambda_{max}(\mu)$, at which the nucleus contains all the mass. In that case, the atmosphere has been ''swallowed'' and the system has the same structure as a cold white dwarf star [14]. This is a relatively singular limit, since the density drops to zero at a finite radius, whereas for partially degenerate systems, the density decays like r^{-2} at large distances. We can study the formation of this compact object by defining an order parameter $\kappa=R_{95}/R$, where R_{95} is the radius of the sphere that contains 95% of the mass [10]. This parameter is ploted as a function of energy in Fig. 12 and the diagram is similar to the one obtained by Follana and Laliena [10] with a different regularization of the potential at the origin. For high energies, the density varies smoothly with the distance and $\kappa\sim 1$. For low energies, the system spontaneously forms a dense core containing more and more mass so that $\kappa\to\kappa_c\ll 1$ [with $\kappa_c\simeq 6.678/\mu^{2/3}$, estimated from the mass-radius relation (33) of a completely degenerate nucleus]. We observe that the order parameter varies rapidly in the region of negative specific heats but remains continuous. According to Cerruti-Sola *et al.* [29], this is the mark of a second order phase transition at $\Lambda=\Lambda_0$ (corresponding to the point of minimum temperature η_c). At that point, the specific heat is infinite and turns from positive to negative; more precisely, $C=dE/dT$ di-

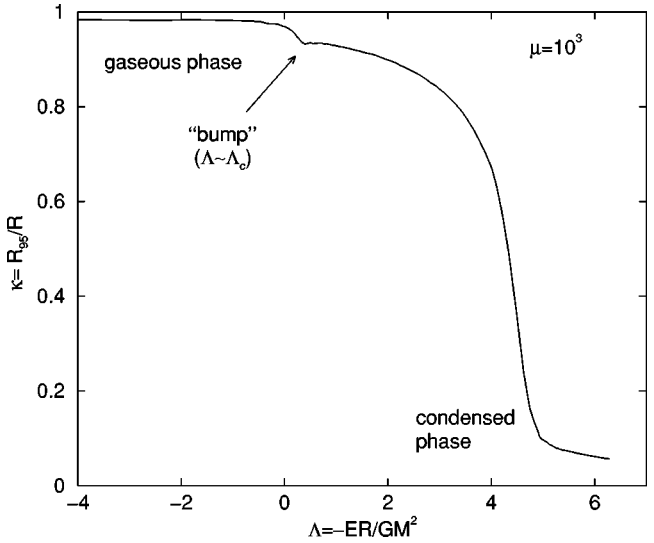

FIG. 12. Evolution of the order parameter with energy for $\mu=10^3$. This figure illustrates the ''clustering'' of the self-gravitating gas as energy is lowered. The presence of the ''bump'' at $\Lambda\sim\Lambda_c$ was previously noted by Follana and Laliena [10] in their model.

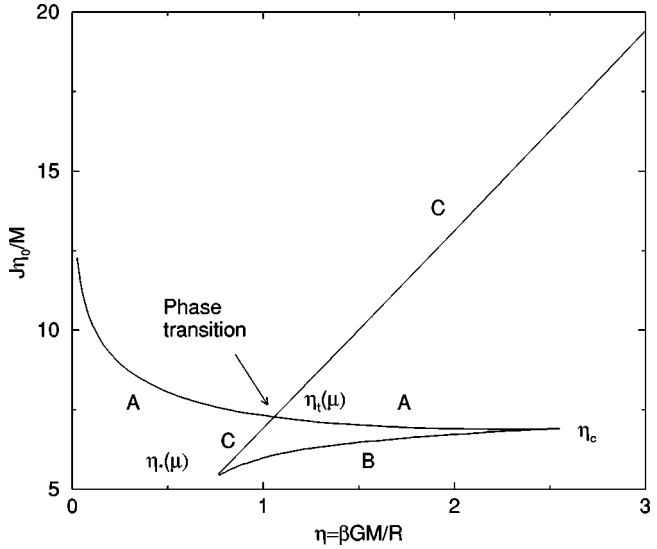

FIG. 13. Free energy of each phase vs inverse temperature for $\mu=10^3$. The interpretation is the same as in Fig. 9.

verges like $(\Lambda-\Lambda_0)^{-1}$ and $\pm(\eta_c-\eta)^{-1/2}$ [25]. In fact, this ''second order phase transition'' is not really a phase transition; it just corresponds to the ''clustering'' of the self-gravitating gas as its energy is progressively reduced.

If we now consider the canonical situation, we see that several solutions exist at the same temperature. A first order phase transition occurs at $\eta_t(\mu)$ and separates a ''gaseous'' phase from a ''condensed'' phase. The interpretation is the same as in the microcanonical ensemble. The energy is discontinuous at the transition so that a large amount of latent heat is released. The specific heat is also discontinuous, but remains positive. For $\eta>\eta_t(\mu)$ the ''gaseous'' states are *metastable* but they probably are physical. This metastable branch completely disapears at $\eta=\eta_c$ and the system undergoes an ''isothermal collapse.'' This phase transition is more radical than the previous one since it is marked by the disapearance of the metastable phase. For self-gravitating fermions the ''isothermal collapse'' ends up on a compact object that contains almost all of the mass (for $\mu=10^3$, $M_*\simeq M$, and $R_*\simeq 6.7\times10^{-2}R$ at $\eta\sim\eta_c$). Since the collapse is marked by a discontinuity of the free energy (see Fig. 13), this could be called a zeroth order phase transition [28]. It has been shown in Ref. [25] that the point of minimum temperature η_c coincides with the Jeans instability criterion. More precisely, the condition of instability of an isothermal gas sphere can be written $R>(\eta_c/3)^{1/2}L_J\sim L_J$, where L_J is the Jeans length. Since $\eta_t<\eta_c$, a first order phase transition can occur at scales much smaller than the Jeans scale ($R=(\eta_t/3)^{1/2}L_J\ll L_J$). This might explain the formation of smaller objects than usually achieved with the ordinary Jeans instability. This idea has been developed by Stahl *et al.* [9] in relation with planet formation. However, the metastable states for $\eta>\eta t$ may be long-lived and it is not clear whether a phase transition will actually occur at η_t.

IV. TRICRITICAL POINTS

We have indicated in the preceding section that the phase transition in the microcanonical ensemble disapears at a critical degeneracy parameter $\mu_{\rm MTP}\simeq 2600$ and that the phase transition in the canonical ensemble disapears for $\mu<\mu_{\rm CTP}\simeq 82.5$. These points at which the Λ-η curve presents an inflexion are called *tricritical points* (TP) in the language of phase transitions.

In Fig. 14, we have enlarged the phase diagram near the tricritical point in the canonical ensemble. It is located at $\Lambda_{\rm CTP}\simeq 0.5$ and $\eta_{\rm CTP}\simeq 3.06$. In the canonical ensemble, the oscillations of the Λ-η curve for $\mu>\mu_{\rm CTP}$ are replaced by a horizontal Maxwell plateau connecting the gaseous phase (left) to the condensed phase (right). This characterizes a canonical first order phase transition at $\eta_t(\mu)$. This diagram exhibits a close analogy with the classical gas-liquid transition, the liquid phase being the counterpart of the (gravitational) Fermi condensate. At the canonical tricritical point CTP the two phases merge, the plateau disappears, and the specific heat diverges like $C\sim(\Lambda-\Lambda_c)^{-2}\sim|\eta-\eta_c|^{-2/3}$. Therefore, the first order phase transition becomes second order at the canonical tricritical point.

The gravitational Fermi gas diagram is nevertheless more complex than the liquid-gas diagram because it presents *another* tricritical point in the microcanonical ensemble (MTP). In Fig. 15, we have enlarged the phase diagram near this tricritical point. It is located at $\Lambda_{\rm MTP}\simeq 0.38$, $\eta_{\rm MTP}\simeq 1.68$. The interpretation is the same as in the canonical ensemble except that the plateau is now vertical as it corresponds to a discontinuity of temperature at a transition energy $\Lambda_t(\mu)$ (microcanonical first order phase transition). We have denoted by η_{gas} and η_{cond} the values of the inverse temperature of the two phases at the transition energy. At the tricritical point $\eta_{gas}=\eta_{cond}$. We have also indicated in the figure the point of minimum temperature η_c at which the specific heat diverges (second order microcanonical phase transition).

In Fig. 16, we have plotted the values of the transition

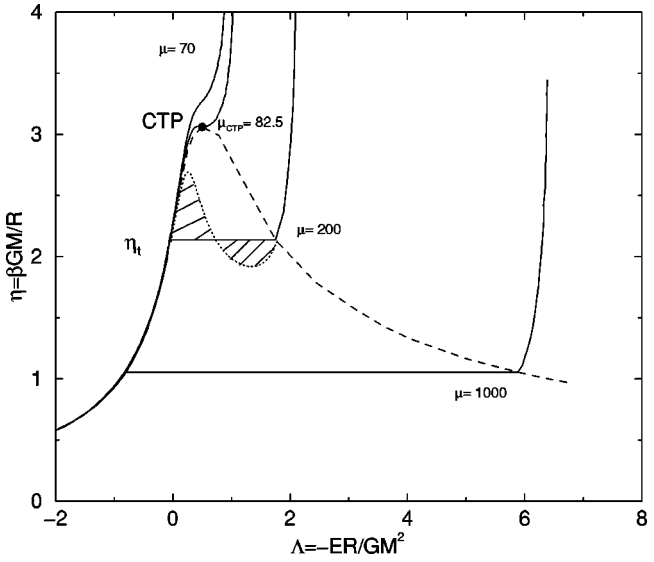

FIG. 14. Enlargement of the phase diagram near the tricritical point in the canonical ensemble. The Maxwell construction determining the transition temperature $\eta_t(\mu)$ is done explicitly (dashed areas). For $\mu_{\mathrm{CTP}}=82.5$ the Maxwell plateau disapears and the Λ-η curve presents an inflexion point at $\Lambda_{\mathrm{CTP}}\simeq 0.5$, $\eta_{\mathrm{CTP}}\simeq 3.06$. At that point, the specific heat becomes infinite and the transition is second order. This diagram is remarkably similar to the liquid-gas transition for an ordinary fluid.

temperature η_t in the canonical ensemble and the values of the characteristic temperatures η_{gas} and η_{cond} in the microcanonical ensemble as a function of the degeneracy parameter μ. These curves characterize first order phase transitions in the canonical and microcanonical ensembles. We have

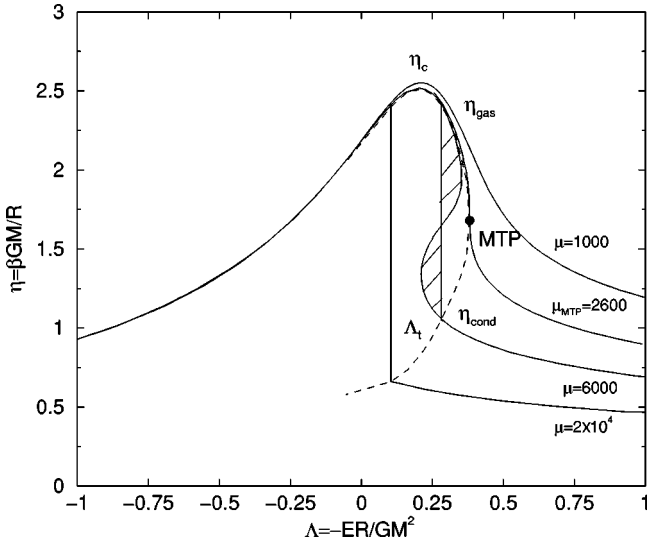

FIG. 15. Enlargement of the phase diagram near the tricritical point in the microcanonical ensemble. The Maxwell construction determining the transition energy $\Lambda_t(\mu)$ is done explicitly (dashed areas). For $\mu_{\mathrm{MTP}}=2600$ the Maxwell plateau disappears and the Λ-η curve presents an inflexion point at $\Lambda_{\mathrm{MTP}}\simeq 0.38$, $\eta_{\mathrm{MTP}}\simeq 1.68$. We have indicated different characteristic temperatures, as described in the text.

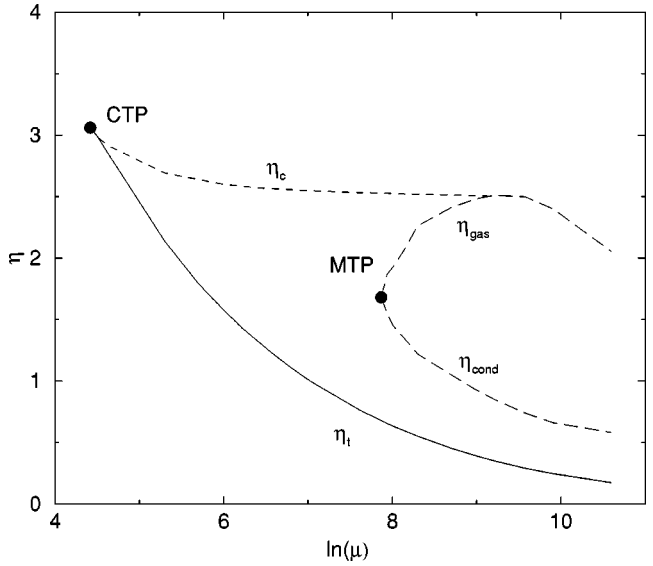

FIG. 16. Phase diagram of the self-gravitating Fermi gas in the μ-η plane. The solid line gives the transition temperature at the canonical first order phase transition. The dashed lines give the temperatures of the two phases (gas and condensate) at the microcanonical first order phase transition. The dotted line gives the critical temperature η_c at the microcanonical second order phase transition. CTP and MTP are the tricritical points in the two ensembles.

also represented the minimum temperature η_c marking the onset of a microcanonical second order phase transition. At the CTP, this branch connects the η_t branch. This is consistent with the appearance of an *isolated* second order phase transition in the canonical ensemble at CTP. This diagram shares some similitudes with the one obtained by Barré *et al.* [12] in their analysis of the BEG model with infinite range interactions. This system also displays an inequivalence of ensembles, regions of negative specific heats, and two tricritical points (one in each ensemble). This analogy suggests that these properties are related to the long-range nature of the interactions more than to the details of the model. This implies a kind of universality for this type of systems. However, there are also noticable differences between the two models. In particular, in the BEG model, second order phase transitions are characterized by a discontinuity of the specific heat (angular point) while in our model of self-gravitating fermions the specific heat is always continuous except at the critical point η_c at which it diverges (this is our definition of a second order phase transition). Therefore, there still exists a second order phase transition above the canonical tricritical point in the BEG model but not in the self-gravitating Fermi gas. Another consequence of the continuity of the specific heats in our model is that the second order critical line $\eta_c - \mu$ (dotted line) does not connect the first order critical lines (dashed lines) at the microcanonical tricritical point MTP but slightly after, unlike in the BEG model [12].

V. A SIMPLE ANALYTICAL MODEL FOR SELF-GRAVITATING FERMIONS

The previous study has revealed that self-gravitating fermions can undergo a phase transition from a ''gaseous''

phase to a ''condensed'' phase. We shall now propose a simple analytical model to describe this phase transition more conveniently. As we shall see, our model can reproduce remarkably well the essential features of the equilibrium phase diagram and it can be used to determine the dependance of the critical parameters on the degeneracy parameter μ.

A. The "gaseous" phase

The ''gaseous'' phase can be represented by a homogeneous distribution of particles with a Maxwellian distribution of velocities

$$f=\frac{\rho}{(2\pi T)^{3/2}}e^{-v^2/2T}. \tag{24}$$

The relation between the energy and the temperature is given by

$$E=\frac{3}{2}MT-\frac{3GM^2}{5R}, \tag{25}$$

and the entropy by

$$\frac{\eta_0 S}{M}=\frac{3}{2}\ln(2\pi T)-\ln\left(\frac{3M}{4\pi R^3}\right)+\ln\eta_0+\frac{3}{2}. \tag{26}$$

Introducing the normalized energy Λ and the normalized temperature η defined in Sec. II B, we can rewrite the previous equations in the form

$$\Lambda=\frac{3}{5}-\frac{3}{2\eta}, \tag{27}$$

$$\frac{\eta_0 S}{M}=-\frac{3}{2}\ln\eta+\ln\mu+\frac{3}{2}+\frac{1}{2}\ln\pi-\ln 6. \tag{28}$$

These equations correctly describe the gaseous phase for high energies and high temperatures (i.e., low density contrasts). Of course, it cannot reproduce the spiral behavior of the classical phase diagram, which is an intrinsic property of the Emden equation. An analytical expression for this spiral has been given in Ref. [25] in the asymptotic limit of high density contrasts.

B. The "condensed" phase

For the ''condensed'' phase, we shall improve the core-halo model proposed by Chavanis and Sommeria [6]. We assume that the ''core'' is completely degenerate and we denote by M_*, R_*, and E_* its mass, radius, and energy, respectively. In that limit, the distribution function is a step function: $f=\eta_0$ for $v\leqslant v_{max}$ and $f=0$ for $v>v_{max}$. Of course, for a self-gravitating system, the maximum velocity v_{max} is a function of the position. For this simple distribution function, the pressure and the density are given by

$$p=\frac{1}{3}\int fv^2 d^3\mathbf{v}=\frac{4\pi\eta_0}{3}\frac{v_{max}^5}{5}, \tag{29}$$

$$\rho=\int f d^3\mathbf{v}=4\pi\eta_0\frac{v_{max}^3}{3}. \tag{30}$$

Eliminating the velocity between these two relations, we find that the equation of state of a completely degenerate system is that of a polytrope with index $\gamma=5/3$ (or $n=3/2$),

$$p=K\rho^{5/3},\quad K=\frac{1}{5}\left(\frac{3}{4\pi\eta_0}\right)^{2/3}. \tag{31}$$

These results are, of course, well known from the theory of white dwarf stars [14] and they are repeated only in order to determine the constant K in the present context. Now, from the theory of polytropic spheres [14], the mass-radius relation is given in the general case by

$$K=N_n GM^{(n-1)/n}R^{(3-n)/n}, \tag{32}$$

where N_n is a constant depending on the index of the polytrope. For $n=3/2$, one has $N_{3/2}=0.42422\ldots$. Therefore, the relation between the mass and the radius of our degenerate nucleus is

$$M_*R_*^3=\frac{\chi}{\eta_0^2 G^3},\quad \text{with}\quad \chi\simeq 5.9723\times 10^{-3}. \tag{33}$$

On the other hand, its energy is given by [14]

$$E_*=-\frac{3}{7}\frac{GM_*^2}{R_*}, \tag{34}$$

and its entropy is equal to zero since the distribution function is unmixed ($f=\eta_0$).

By shrinking, the nucleus releases an enormous amount of energy that heats the envelope. The envelope behaves therefore like an ordinary gas maintained by the walls of the box so that its density is approximately uniform. Its energy and entropy are therefore given by

$$E_{halo}=\frac{3}{2}(M-M_*)T-\frac{3GM_*(M-M_*)}{2R}-\frac{3G(M-M_*)^2}{5R}, \tag{35}$$

$$\eta_0 S=(M-M_*)[\tfrac{3}{2}\ln(2\pi T)-\ln(M-M_*)+\ln V+\ln\eta_0+\tfrac{3}{2}]. \tag{36}$$

Contrary to our previous paper [6], we have not neglected the potential energy of the envelope as compared to its thermal energy. This sensibly improves the agreement with the full numerical solution. However, we have still assumed that the core is much smaller than the halo, so that $V=\frac{4}{3}\pi R^3$ represents the total volume of the system. For calculating the potential energy, we have used the formula

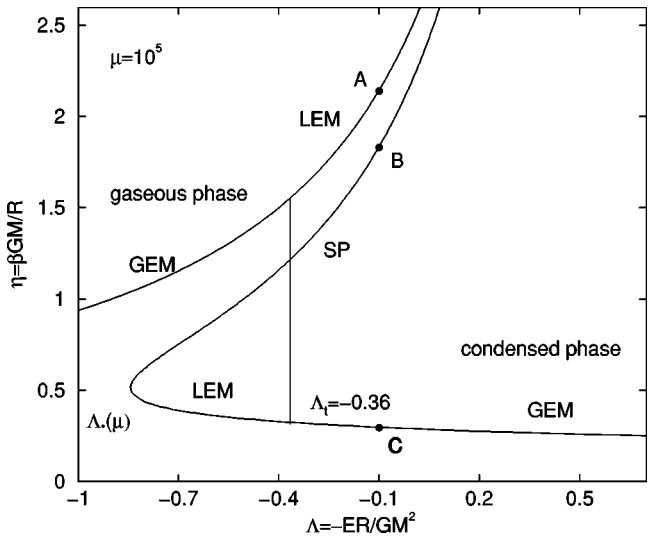

FIG. 17. Equilibrium phase diagram obtained from our analytical model ($\mu=10^5$). It compares relatively well with the full numerical solution reported in Fig. 7.

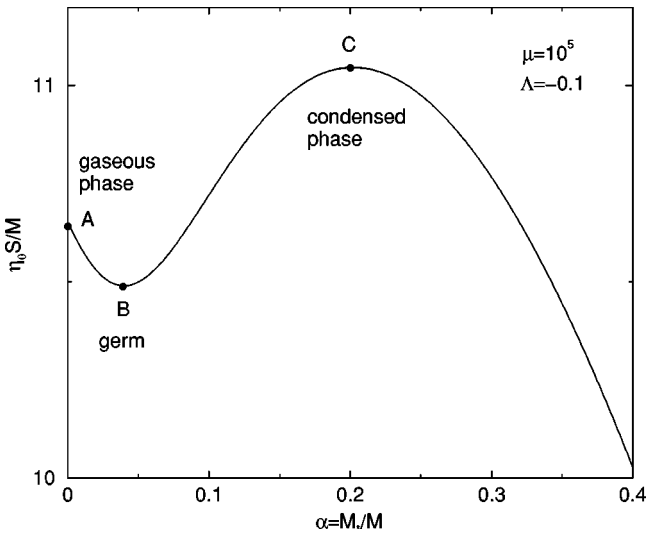

FIG. 18. Entropy as a function of the mass of the nucleus for $\mu=10^5$ and $\Lambda=-0.1>\Lambda_t$. This curve is obtained by using the analytical formulas (41)–(43). For $\Lambda>\Lambda_t$, the "condensed" state (point C) is a global entropy maximum and the "gaseous" state (point A) a local entropy maximum. The solution with the "germ" (point B) is an entropy minimum. The fraction of mass contained in the nucleus is relatively large for $\mu=10^5$ (see Fig. 19) but it decreases as the classical limit is approached. As $\mu\to+\infty$, $\alpha_{cond}\to 0$, $\alpha_{germ}\to 0$ with $\alpha_{cond}\gg\alpha_{germ}$.

$$W=-4\pi G\int \rho M(r) r dr, \tag{37}$$

where $M(r)$ is the mass contained within the sphere of radius r. This formula is valid for an arbitrary spherically symmetrical distribution of matter [22].

Adding Eqs. (34) and (35) and expressing the radius of the core as a function of its mass, using Eq. (33), the total energy of the system is given by

$$E=-\frac{3}{7}\frac{\eta_0^{2/3}G^2}{\chi^{1/3}}M_*^{7/3}+\frac{3}{2}(M-M_*)T - \frac{3GM_*(M-M_*)}{2R}-\frac{3G(M-M_*)^2}{5R}. \tag{38}$$

For a given value of energy (microcanonical ensemble), this relation determines the temperature T as a function of the core mass. Therefore, the entropy (36) is a function of M_* alone. The mass of the nucleus at equilibrium is determined by maximizing the entropy with respect to M_*. After simplification, the condition $dS/dM_*=0$ is found to be equivalent to

$$\ln(M-M_*)+\frac{3G}{2RT}(M-2M_*)-\frac{6G}{5RT}(M-M_*)-\frac{3}{2}\ln T + \frac{G^2\eta_0^{2/3}}{\chi^{1/3}}\frac{M_*^{4/3}}{T}=\ln\eta_0+\ln V-1+\frac{3}{2}\ln(2\pi). \tag{39}$$

We obtain the same relation by maximizing the free energy J at fixed mass and temperature. Equations (38) and (39) completely determine the equilibrium phase diagram of self-gravitating fermions in the framework of our analytical model. For convenience, we shall reexpress these equations in a dimensionless form. To that purpose, we introduce the fraction of mass α contained in the core such that $M_*=\alpha M$. In terms of α, the radius of the core is $R_*/R=6.678\alpha^{-1/3}\mu^{-2/3}$ [see Eq. (33)]. On the other hand, we set

$$\lambda=\frac{1}{(512\pi^4\chi)^{1/3}}=0.149756\ldots,$$
$$C=\frac{1}{2}\ln\pi-\ln 6-1=-2.21939\ldots. \tag{40}$$

Introducing furthermore the dimensionless energy Λ and the dimensionless temperature η defined in Sec. II B, the equations of the problem become

$$\Lambda=\frac{3}{7}\lambda\mu^{2/3}\alpha^{7/3}-\frac{3}{2}(1-\alpha)\frac{1}{\eta}+\frac{3}{2}\alpha(1-\alpha)+\frac{3}{5}(1-\alpha)^2, \tag{41}$$

$$\ln(1-\alpha)+\tfrac{3}{2}\ln\eta+\lambda\mu^{2/3}\alpha^{4/3}\eta+\tfrac{9}{5}\eta(\tfrac{1}{6}-\alpha)=\ln\mu+C, \tag{42}$$

$$\frac{\eta_0 S}{M}=(1-\alpha)\left[-\frac{3}{2}\ln\eta-\ln(1-\alpha)+\ln\mu+C+\frac{5}{2}\right], \tag{43}$$

$$\frac{\eta_0 J}{M}=\frac{\eta_0 S}{M}+\eta\Lambda. \tag{44}$$

The equilibrium phase diagram is represented in Fig. 17 for a degeneracy parameter $\mu=10^5$. It provides a fairly good agreement with the full numerical solution of Sec. II B (see Fig. 7). Of course, we cannot expect to reproduce exactly the

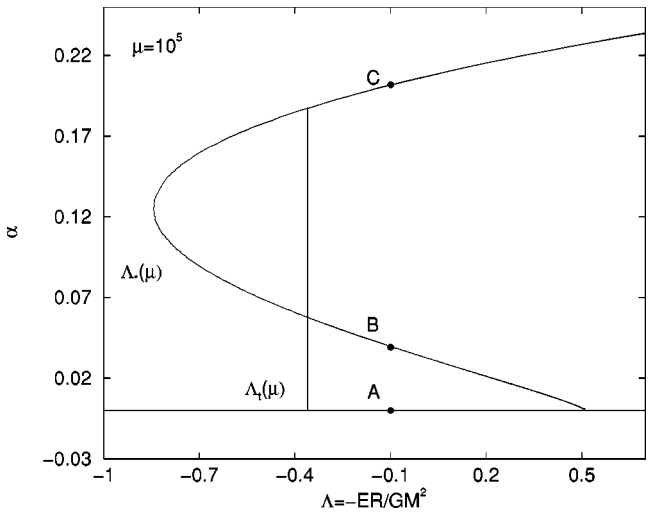

FIG. 19. Evolution of the fraction of mass contained in the nucleus as a function of energy for a degeneracy parameter $\mu=10^5$.

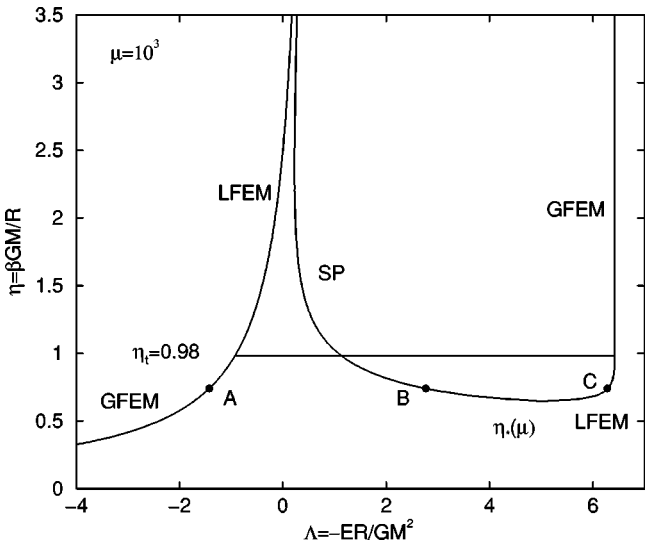

FIG. 20. Equilibrium phase diagram obtained from our analytical model ($\mu=10^3$). It compares relatively well with the full numerical solution reported in Fig. 10.

numerical results in view of the approximations made in our analytical model. In particular, except for very low energies, the core is only partially degenerate and this is responsible for the quantitative discrepencies observed between the two diagrams. However, the qualitative behavior is the same and this is essentially what was attempted by our analytical approach. In particular, we recover the three types of solutions previously studied. The solutions on the upper branch (points *A*) form the ''gaseous'' phase. They can also be considered as a particular limit of the core-halo model with $\alpha=0$. The solutions on the lower branch (points *C*) form the ''condensed'' phase and the solutions on the intermediate branch (points *B*) are similar to the ''gaseous'' states (points *A*) except that they possess a small central nucleus (a ''germ''). To determine the stability of these solutions we have ploted in Fig. 18 their entropy as a function of the core mass α for a given energy. The curve $S(\alpha)$ has the usual ''W shape'' characteristic of phase transitions. The ''gaseous'' state ($\alpha=0$) can be considered as an entropy maximum although it does not correspond to the condition $dS/d\alpha=0$. The other entropy maximum corresponds to the ''condensed'' state (point *C*) and the entropy minimum to the solution with the germ (point *B*). For $\Lambda>\Lambda_t$, the ''condensed'' states *C* are global entropy maxima and the ''gaseous'' states *A* are local entropy maxima (the reverse is true for $\Lambda<\Lambda_t$). However, to pass from *A* to *C*, we have to cross an entropic barrier constituted by the solution *B*. This requires that the entropy *decreases*, which is not possible for an isolated system. Therefore, depending on whether the initial fraction of mass α_0 is smaller or larger than α_{germ}, the system will either relax towards the ''gaseous'' state or collapse towards the ''condensed'' state. Of course, this argument assumes that α is the only degree of freedom in the system, which is clearly an idealization. As mentioned previously, the real ''basin of attraction'' is much more complicated.

The equilibrium phase diagram corresponding to a degeneracy parameter $\mu=10^3$ is represented in Fig. 20 and it compares relatively well with the full numerical solution (see Fig. 10). The minimum energy, corresponding to $\Lambda_{max}(\mu)$, is reached when all the mass is in the degenerate core at zero temperature ($\alpha\to 1$, $\eta\to+\infty$). Equation (41) then yields

$$\Lambda_{max}(\mu)=\frac{3}{7}\lambda\mu^{2/3}. \tag{45}$$

For $\Lambda\to\Lambda_{max}(\mu)$ and for sufficiently large μ, one has

$$1-\alpha\sim e^{-\lambda\mu^{2/3}\eta}, \quad \Lambda_{max}-\Lambda\sim\lambda\mu^{2/3}e^{-\lambda\mu^{2/3}\eta}. \tag{46}$$

This shows that the atmosphere is swallowed exponentially rapidly when we approach the minimum energy. Figure 20 displays a clear phase transition in the canonical ensemble. The value of the temperature of transition is very close to the exact value found in the numerical approach. In the present case, we can safely consider that the core of the condensate is completely degenerate so that the quantitative agreement with the exact solution is better than in the microcanonical ensemble. Once again, the stability of the equilibrium states can be determined by considering the variation of the free energy with the core mass (see Fig. 21). For $\eta<\eta_t$ ($\eta>\eta_t$), the ''gaseous'' state is a global (local) maximum of free energy and the ''condensed'' state a local (global) one. The description of the phase transition is the same as in the microcanonical ensemble.

C. Scaling laws in the limit $\mu\to+\infty$

We shall now determine the behavior of the critical parameters as $\mu\to+\infty$ (classical limit). In the microcanonical ensemble, the phase transition occurs close to the maximum energy E_* of the condensed phase, corresponding to $\Lambda_*(\mu)$. Using Eqs. (41) and (42), we find that the condition of energy maximum $d\Lambda=0$ is equivalent to

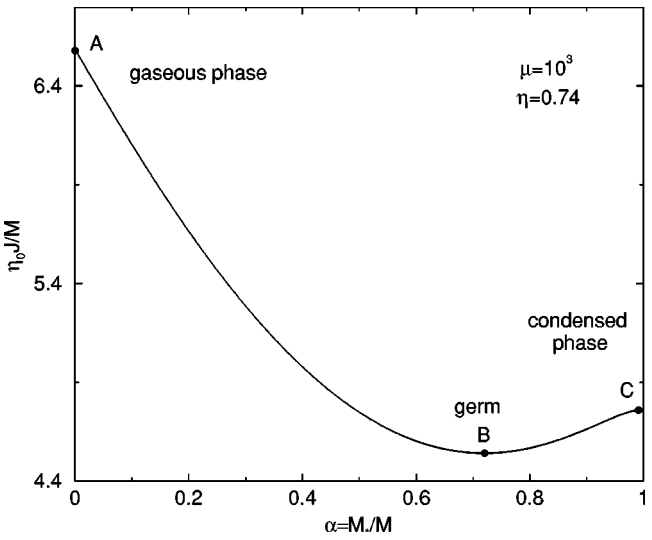

FIG. 21. Free energy as a function of the mass of the nucleus for $\mu=10^3$ and $\eta=0.74<\eta_t$. For $\eta<\eta_t$, the ''gaseous'' state is a global maximum of free energy and the ''condensed'' state is a local maximum of free energy. The solution with the ''germ'' is a minimum of free energy. The fraction of mass contained in the condensate is close to one (see Fig. 22). In the limit $\mu\to\infty$, $\alpha_{cond}\to 1$, and $\alpha_{germ}\to 0$.

$$\left[\frac{3}{2}+\lambda\mu^{2/3}\alpha^{4/3}\eta+\frac{9}{5}\eta\left(\frac{1}{6}-\alpha\right)\right]^2 = \frac{3}{2}(1-\alpha)\left(\frac{4}{3}\lambda\mu^{2/3}\alpha^{1/3}\eta-\frac{1}{1-\alpha}-\frac{9}{5}\eta\right). \tag{47}$$

This equation, together with Eqs. (41) and (42), determines the function $\Lambda_*(\mu)$. Now, in the limit $\mu\to+\infty$, the fraction of mass contained in the nucleus goes to zero while the temperature increases. Taking the limit $\mu\to+\infty$, $\alpha\to 0$, and $\eta\to 0$ in Eq. (47), we obtain the relation

$$\lambda\mu^{2/3}\alpha^{7/3}\eta=2. \tag{48}$$

Considering the limiting form of Eqs. (41) and (42) in the same approximation, we find

$$\Lambda=\frac{3}{7}\lambda\mu^{2/3}\alpha^{7/3}-\frac{3}{2\eta}, \tag{49}$$

$$\tfrac{3}{2}\ln\eta+\lambda\mu^{2/3}\alpha^{4/3}\eta=\ln\mu. \tag{50}$$

Therefore, the thermodynamical parameters at the point of maximum energy behave with the degeneracy parameter like

$$\alpha_*\sim\frac{1}{\ln\mu},\quad \eta_*\sim\frac{(\ln\mu)^{7/3}}{\mu^{2/3}},\quad \Lambda_*\sim-\frac{\mu^{2/3}}{(\ln\mu)^{7/3}}. \tag{51}$$

The transition point $\Lambda_t(\mu)$ is determined by equating the entropy of the two phases. This yields

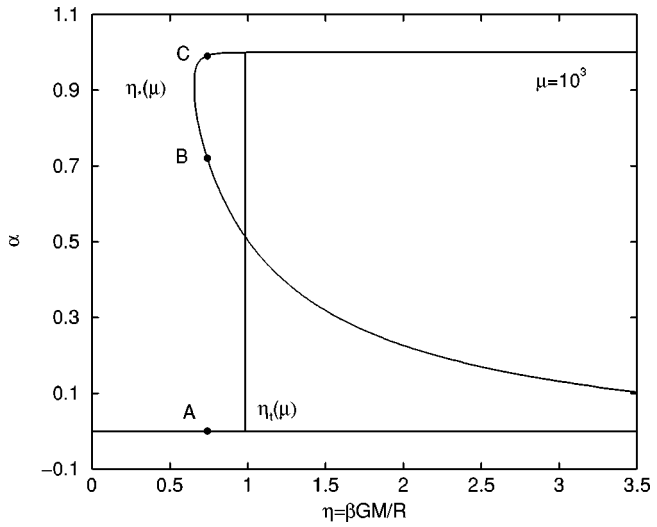

FIG. 22. Evolution of the fraction of mass contained in the nucleus as a function of the inverse temperature for a degeneracy parameter $\mu=10^3$.

$$(1-\alpha)[-\tfrac{3}{2}\ln\eta_{cond}-\ln(1-\alpha)+\ln\mu+C+\tfrac{5}{2}] = -\tfrac{3}{2}\ln\eta_{gas}+\ln\mu+C+\tfrac{5}{2}, \tag{52}$$

where η_{cond} is the temperature of the condensed phase, η_{gas} the temperature of the gaseous phase, and α the mass contained in the condensate at the transition point. Considering the limiting form of Eqs. (27), (41), and (42), when $\mu\to+\infty$, $\alpha\to 0$, and $\eta\to 0$, we find that

$$\Lambda=-\frac{3}{2\eta_{gas}}=\frac{3}{7}\lambda\mu^{2/3}\alpha^{7/3}-\frac{3}{2\eta_{cond}}, \tag{53}$$

$$\tfrac{3}{2}\ln\eta_{cond}+\lambda\mu^{2/3}\alpha^{4/3}\eta_{cond}=\ln\mu. \tag{54}$$

Solving for η_{cond} and η_{gas}, we get

$$\eta_{cond}\sim\frac{2\ln\mu}{\lambda\mu^{2/3}\alpha^{4/3}},\quad \frac{1}{\eta_{gas}}\sim\frac{\lambda\mu^{2/3}\alpha^{4/3}}{2\ln\mu}\left(1-\frac{4}{7}\alpha\ln\mu\right). \tag{55}$$

Substituting these results in Eq. (52), we find that the mass contained in the condensate behaves like

$$\alpha\sim\frac{1}{\ln\mu}. \tag{56}$$

Combining the foregoing relations, we find that the energy of transition is given by

$$\Lambda_t\sim-\frac{\mu^{2/3}}{(\ln\mu)^{7/3}}. \tag{57}$$

In the classical limit, $\Lambda_t\to-\infty$, so that the ''gaseous'' states are always metastable as previously discussed. The temperatures of the two phases at the transition point behave like

$$\eta_{gas} \sim \eta_{cond} \sim \frac{(\ln \mu)^{7/3}}{\mu^{2/3}}. \quad (58)$$

The jump of temperature is given by

$$\frac{1}{\eta_{cond}} - \frac{1}{\eta_{gas}} \sim \frac{\mu^{2/3}}{(\ln \mu)^{7/3}}. \quad (59)$$

Finally, we can study the behavior of the fraction of mass contained in the germ and in the condensate as $\mu \to +\infty$ for a given value of energy Λ. For the condensate (points C), $\alpha \to 0$ and $\eta \to 0$ so that Eqs. (41) and (42) simplify in

$$\frac{3}{2\eta} = \frac{3}{7}\lambda \mu^{2/3} \alpha^{7/3}, \quad (60)$$

$$\frac{3}{2} \ln \eta + \lambda \mu^{2/3} \alpha^{4/3} \eta = \ln \mu. \quad (61)$$

The first equality simply means that the potential energy of the core tends to $-\infty$ so that the temperature of the halo must rise to $+\infty$ so as to maintain the total energy fixed. Combining Eqs. (60) and (61) using Eq. (43), we obtain

$$\alpha_{cond} \sim \frac{1}{\ln \mu}, \quad \eta_{cond} \sim \frac{(\ln \mu)^{7/3}}{\mu^{2/3}}, \quad S_{cond} \sim \ln \mu. \quad (62)$$

Since the entropy diverges as $\mu \to +\infty$, we recover the well-known fact that there is no global entropy maximum for a classical self-gravitating gas. Note that the divergence of entropy is relatively slow (logarithmic). For the germ (points B), we have in the classical limit

$$\alpha_{germ} \to 0, \quad \eta_{germ} \to \eta_{gas}, \quad S_{germ} \to S_{gas}. \quad (63)$$

These results simply reflect the fact that the unstable branch approaches the gaseous branch as $\mu \to +\infty$ but still differs from it by a presence of a small germ. The size of the germ is determined by Eq. (42). For $\mu \to +\infty$, it leads to

$$\lambda \mu^{2/3} \alpha^{4/3} \eta_{gas} = \ln \mu \quad (64)$$

so that

$$\alpha_{germ} \sim \frac{(\ln \mu)^{3/4}}{\mu^{1/2}}. \quad (65)$$

For a given energy, the mass contained in the condensate and in the germ goes to zero as we approach the classical limit. However, the relation

$$\frac{\alpha_{germ}}{\alpha_{cond}} \sim \frac{(\ln \mu)^{7/4}}{\mu^{1/2}} \ll 1 \quad (66)$$

indicates that the size of the germ is much smaller than the size of the condensate.

These results are consistent with the proof given in Ref. [26] for the absence of global entropy maximum in the microcanonical ensemble. We can make the entropy diverge by approaching an arbitrarily small fraction of particles in the core ($M_* \ll M$) so that the potential energy goes to $-\infty$. Since the total energy is conserved, the temperature must rise to $+\infty$ and this leads to a logarithmic divergence of the entropy. This ''natural'' evolution (in a thermodynamical sense) is confirmed by dynamical models of self-gravitating systems (see the discussion in Ref. [26]). It is found that the gravitational collapse of classical point masses leads to a finite time singularity (the central density becomes infinite in a finite time t_{coll}) with a slow algebraic divergence of the temperature and a logarithmic divergence of the entropy as $t \to t_{coll}$. In addition, the mass contained in the core tends to zero as $t \to t_{coll}$ (the density profile at $t = t_{coll}$ is close to a power law $\rho \simeq r^{-\alpha}$, with $\alpha \simeq 2.2 < 3$) in agreement with our previous observations.

We now consider the canonical situation. In the limit $\mu \to +\infty$, the phase transition occurs close to maximum temperature of the condensed phase, corresponding to $\eta_*(\mu)$. Using Eq. (42), we find that the condition of temperature maximum $d\eta = 0$ is equivalent to

$$\frac{4}{3}\lambda \mu^{2/3} \alpha^{1/3} \eta - \frac{1}{1-\alpha} - \frac{9}{5}\eta = 0. \quad (67)$$

This equation, together with Eq. (42), determines the function $\eta_*(\mu)$. In the limit $\mu \to +\infty$, the fraction of mass contained in the condensate comes close to unity and the maximum temperature increases. Taking the limit $\alpha \to 1$ and $\eta \to 0$ in Eq. (67), we get

$$\frac{4}{3}\lambda \mu^{2/3} \eta = \frac{1}{1-\alpha}. \quad (68)$$

Simplifying Eqs. (41) and (42) in the same approximation, we obtain

$$\Lambda = \frac{3}{7}\lambda \mu^{2/3} - \frac{3}{2}(1-\alpha)\frac{1}{\eta}, \quad (69)$$

$$\ln(1-\alpha) + \tfrac{3}{2} \ln \eta + \lambda \mu^{2/3} \eta = \ln \mu. \quad (70)$$

We find, therefore, that the parameters at the point of maximum temperature behave like

$$1 - \alpha_* \sim \frac{1}{\ln \mu}, \quad \eta_* \sim \frac{\ln \mu}{\mu^{2/3}}, \quad \Lambda_* - \Lambda_{max}(\mu) \sim -\frac{\mu^{2/3}}{(\ln \mu)^2}. \quad (71)$$

The transition point $\eta_t(\mu)$ in the canonical ensemble is obtained by equating the free energy of the two phases. Using the results of Secs. V A and Sec. V B we obtain the general relation

$$-\tfrac{3}{2} \ln \eta + \ln \mu + C + 1 + \tfrac{3}{5}\eta$$
$$= (1-\alpha)[-\tfrac{3}{2} \ln \eta - \ln(1-\alpha) + \ln \mu + C + \tfrac{5}{2}]$$
$$+ \tfrac{3}{7}\lambda \eta \mu^{2/3} \alpha^{7/3} - \tfrac{3}{2}(1-\alpha) + \tfrac{3}{2}\eta\alpha(1-\alpha) + \tfrac{3}{5}\eta(1-\alpha)^2, \quad (72)$$

where α is the mass contained in the condensate at the transition point. In the limit $\mu\to+\infty$ and $\alpha\to 1$, this relation reduces to

$$-\tfrac{3}{2}\ln\eta+\ln\mu=\tfrac{3}{7}\eta\lambda\mu^{2/3}. \tag{73}$$

The free energy of the gaseous phase (left-hand side) is dominated by the contribution of the entropy and the free energy of the condensed phase (right-hand side) is dominated by the energy of the core. We find, therefore, that the temperature of the transition behaves like

$$\eta_t\sim\frac{\ln\mu}{\mu^{2/3}}. \tag{74}$$

The mass contained in the condensate is determined by Eq. (42). In the limit $\mu\to+\infty$, it simplifies to

$$\ln(1-\alpha)+\tfrac{3}{2}\ln\eta+\lambda\mu^{2/3}\eta=\ln\mu. \tag{75}$$

Solving for α in Eqs. (73) and (75), we get

$$1-\alpha\sim\frac{1}{\mu^{8/3}}. \tag{76}$$

According to Eqs. (27), (41), and (74), the energy of the gaseous phase and the energy of the condensed phase behave at the transition point like

$$\Lambda_{gas}\sim-\frac{\mu^{2/3}}{\ln\mu},\quad \Lambda_{cond}-\Lambda_{max}(\mu)\sim-\frac{1}{\mu^2\ln\mu}. \tag{77}$$

The jump in the energy (latent heat) is

$$\Lambda_{cond}-\Lambda_{gas}\sim\mu^{2/3}\left(1+\frac{3}{4\ln\mu}\right). \tag{78}$$

Finally, let us determine the fraction of mass contained in the condensate and in the germ as $\mu\to+\infty$ for a given value of temperature. For the condensate (points C), $\alpha\to 1$ so that Eq. (42) leads to

$$1-\alpha_{cond}\sim e^{-\lambda\eta\mu^{2/3}}. \tag{79}$$

The free energy of the condensed state behaves like

$$J\sim\Lambda_{max}(\mu)\,\eta\sim\mu^{2/3}. \tag{80}$$

The divergence of the free energy in the canonical ensemble is more rapid than the divergence of the entropy in the microcanonical ensemble. This is simply because the free energy is dominated by the divergence of the (potential) energy while the entropy is dominated by the divergence of the logarithm of the temperature. For the germ (points B), we have in the classical limit

$$\alpha_{germ}\to 0,\quad \Lambda\to\Lambda_{gas},\quad J\to J_{gas}. \tag{81}$$

Using Eq. (42), we find that

$$\alpha_{germ}\sim\frac{(\ln\mu)^{3/4}}{\mu^{1/2}}. \tag{82}$$

In the limit $\mu\to+\infty$, the germ contains almost no mass while the condensate contains almost all the mass.

These results again agree with the proof given in Ref. [25] for the absence of a global maximum of free energy in the canonical ensemble. We can make the free energy diverge by collapsing the mass M to a point (the divergence of J is simply due to the divergence of the potential energy; the entropy has a weak, logarithmic, negative divergence). This argument would suggest that the natural evolution of a system of classical point masses in the canonical ensemble is to develop a density profile in the form of a δ function with all the mass at $r=0$. This is *not* what numerical simulations of gravitational collapse show (see the discussion in Ref. [26]). It is usually found that when the system is held at a fixed temperature, the self-similar collapse leads to a density profile close to the power law $\rho\sim r^{-2}$ at $t=t_{coll}$. This profile has a vanishing mass at $r=0$ and its free energy is not divergent. Therefore, a finite time singularity prevents the system from reaching arbitrarily large values of the free energy. It is not known whether other solutions of these dynamical equations (not necessarily self-similar) can lead to the expected δ function with $J=+\infty$.

VI. CLASSICAL GAS WITH A SHORT DISTANCE CUT-OFF

The case of a self-gravitating gas with a short distance cut-off was first considered by Aronson and Hansen [8] and more recently by Stahl *et al.* [9] (see the discussion in Sec. VII D). The equilibrium phase diagram of this system is similar to the one obtained for self-gravitating fermions (see Figs. 7–10). Indeed, the degeneracy parameter μ plays the same role as the inverse of the short distance cut-off a. The interpretation of the phase transitions is therefore similar but the dependance of the critical parameters on the cutoff is different. We shall therefore reformulate our analytical model to the case of a classical hard-sphere gas and determine how the previous results are modified in this new situation.

A. The "gaseous" phase

We model the gaseous phase by a uniform distribution of matter occupying the whole container. The energy and the entropy are, therefore, given by

$$E=\frac{3}{2}NT-\frac{3GM^2}{5R}, \tag{83}$$

$$S/N=\frac{3}{2}+\frac{3}{2}\ln\left(\frac{2\pi T}{m}\right)-\ln\left(\frac{3N}{4\pi R^3}\right). \tag{84}$$

In dimensionless variables, these equations can be rewritten as

$$\Lambda=\frac{3}{5}-\frac{3}{2\eta}, \tag{85}$$

$$S/N=-\frac{3}{2}\ln\eta. \tag{86}$$

In the expression (86) for the entropy, we have not written the constant term

$$\frac{3}{2}+\frac{3}{2}\ln(2\pi)+\ln\left[\frac{4\pi R^3}{3N}\left(\frac{GM}{R}\right)^{3/2}\right], \tag{87}$$

which plays no role in the problem.

B. The "condensed" phase

We model the ''condensed'' phase by a nucleus and an atmosphere, each of uniform density. The velocity distribution of the particles is assumed to be Maxwellian with temperature T. Let R_* be the radius of the nucleus and N_* the number of particles that it contains. We introduce an excluded volume $\sim\frac{4}{3}\pi a^3$ around each particle, where a can be regarded as the ''effective'' size of the particles. R_* and N_* are, therefore, related to each other by a relation of the form

$$R_*^3=4gN_*a^3, \tag{88}$$

where g is a geometrical factor with order of magnitude unity that depends on the nature of the close packing (see Ref. [8]). The energy of the core is

$$E_*=\frac{3}{2}N_*T-\frac{3GM_*^2}{5R_*}, \tag{89}$$

and its entropy

$$S_*=N_*\left[\frac{3}{2}+\frac{3}{2}\ln\left(\frac{2\pi T}{m}\right)-\ln\left(\frac{3N_*}{4\pi R_*^3}\right)\right]. \tag{90}$$

For the halo, we have

$$E_{halo}=\frac{3}{2}(N-N_*)T-\frac{3GM_*(M-M_*)}{2R}-\frac{3G(M-M_*)^2}{5R}, \tag{91}$$

$$S_{halo}=(N-N_*)\left\{\frac{3}{2}+\frac{3}{2}\ln\left(\frac{2\pi T}{m}\right)-\ln\left[\frac{3(N-N_*)}{4\pi R^3}\right]\right\}. \tag{92}$$

As in the case of fermions, we have considered that the volume of the nucleus is much smaller than the volume of the halo. Adding these expressions and using Eq. (88) to express the radius of the core as a function of its mass $M_*=N_*m$, we obtain for the whole configuration

$$E=\frac{3}{2}NT-\frac{3Gm^{1/3}M_*^{5/3}}{5a}-\frac{3GM_*(M-M_*)}{2R}-\frac{3G(M-M_*)^2}{5R}, \tag{93}$$

$$S=N\left[\frac{3}{2}+\frac{3}{2}\ln\left(\frac{2\pi T}{m}\right)-\ln\left(\frac{3N}{4\pi R^3}\right)\right]-N_*\ln\left(\frac{R^3}{Na^3}\right)-(N-N_*)\ln\left(\frac{N-N_*}{N}\right). \tag{94}$$

Let $\alpha=M_*/M$ denote the fraction of mass contained in the nucleus. We also introduce the filling factor

$$\mu=\frac{R}{a(4gN)^{1/3}}, \tag{95}$$

which can be regarded as an inverse normalized hard-sphere radius. The case of point masses corresponds to the limit $\mu\to+\infty$. Clearly, μ plays the same role as the degeneracy parameter in Sec. II B. In dimensionless form, the equations of the problem become

$$\Lambda=-\frac{3}{2\eta}+\tfrac{3}{5}\mu\alpha^{5/3}+\tfrac{3}{2}\alpha(1-\alpha)+\tfrac{3}{5}(1-\alpha)^2, \tag{96}$$

$$S/N=-\tfrac{3}{2}\ln\eta-3\alpha\ln\mu-(1-\alpha)\ln(1-\alpha), \tag{97}$$

where we have again eliminated the constant (87) from the expression of the entropy. We now determine the mass of the nucleus by maximizing the entropy (97) at fixed energy. This yields the relation

$$1+\ln(1-\alpha)-3\ln\mu=-\frac{3\eta}{10}+\frac{9}{5}\alpha\eta-\mu\eta\alpha^{2/3}. \tag{98}$$

Equations (96)–(98) determine the equilibrium phase diagram of a classical hard-sphere gas in the framework of our analytical model. The description of this diagram (and its dependance on the parameter μ) is similar to the one given in Sec. V for self-gravitating fermions. The minimum energy corresponds to the configuration for which all the mass is in the nucleus at zero temperature. Taking the limit $\alpha\to1$ and $\eta\to+\infty$ in Eq. (96), we get

$$\Lambda_{max}(\mu)=\tfrac{3}{5}\mu. \tag{99}$$

For $\Lambda\to\Lambda_{max}$ and for sufficiently large values of μ, Eqs. (96) and (98) yield

$$1-\alpha\sim e^{-\mu\eta},\quad \Lambda_{max}-\Lambda\sim\frac{3}{2\eta}. \tag{100}$$

Note that the relation between the temperature and the energy is different from the corresponding one for self-gravitating fermions [see Eq. (46)].

C. Scaling laws in the limit $\mu\to+\infty$

The derivation of the scaling laws for the critical parameters of a classical hard-sphere gas is essentially the same as for self-gravitating fermions (Sec. V C). We shall directly give the results without detailed discussion.

In the microcanonical ensemble, the point of maximum energy, corresponding to $\Lambda_*(\mu)$, is determined by the relation

$$\frac{2}{3}\eta^2\left(\frac{3}{10}-\frac{9}{5}\alpha+\mu\alpha^{2/3}\right)^2=\frac{2}{3}\mu\eta\alpha^{-1/3}-\frac{9}{5}\eta-\frac{1}{1-\alpha}. \tag{101}$$

In the limit $\mu\to+\infty$, the thermodyanical parameters behave at the point of maximum energy like

$$\alpha_*\sim\frac{1}{\ln\mu},\quad \eta_*\sim\frac{(\ln\mu)^{5/3}}{\mu},\quad \Lambda_*\sim-\frac{\mu}{(\ln\mu)^{5/3}}. \tag{102}$$

At the transition point $\Lambda_t(\mu)$, the equality of the entropy of the two phases leads to the relation

$$-\tfrac{3}{2}\ln\eta_{cond}-3\alpha\ln\mu-(1-\alpha)\ln(1-\alpha)=-\tfrac{3}{2}\ln\eta_{gas}. \tag{103}$$

In the limit $\mu\to+\infty$, the fraction of mass contained in the condensate behaves like

$$\alpha\sim\frac{1}{\ln\mu}. \tag{104}$$

The energy of the transition and the temperature of each phase are given by

$$\Lambda_t\sim-\frac{\mu}{(\ln\mu)^{5/3}},\quad \eta_{gas}\sim\eta_{cond}\sim\frac{(\ln\mu)^{5/3}}{\mu}. \tag{105}$$

The jump in the temperature at the transition point is

$$\frac{1}{\eta_{cond}}-\frac{1}{\eta_{gas}}\sim\frac{\mu}{(\ln\mu)^{5/3}}. \tag{106}$$

For a given energy, the thermodynamical parameters of the condensate behave, in the limit $\mu\to+\infty$, like

$$\alpha_{cond}\sim\frac{1}{\ln\mu},\quad \eta_{cond}\sim\frac{(\ln\mu)^{5/3}}{\mu},\quad S_{cond}\sim\ln\mu. \tag{107}$$

For the germ, we have

$$\alpha_{germ}\sim\left(\frac{\ln\mu}{\mu}\right)^{3/2},\quad \eta_{germ}\to\eta_{gas},\quad S_{germ}\to S_{gas}. \tag{108}$$

In the canonical ensemble, the maximum temperature of the condensed phase, corresponding to $\eta_*(\mu)$, is determined by the relation

$$\frac{2}{3}\mu\eta\alpha^{-1/3}-\frac{1}{1-\alpha}-\frac{9}{5}\eta=0. \tag{109}$$

In the limit $\mu\to+\infty$, the thermodyanical parameters behave at the point of maximum temperature like

$$1-\alpha_*\sim\frac{1}{\ln\mu},\quad \eta_*\sim\frac{\ln\mu}{\mu},\quad \Lambda_*-\Lambda_{max}(\mu)\sim-\frac{\mu}{\ln\mu}. \tag{110}$$

At the transition point $\eta_t(\mu)$, the equality of the free energy of the two phases yields

$$\tfrac{3}{5}\eta=-3\alpha\ln\mu-(1-\alpha)\ln(1-\alpha)+\tfrac{3}{5}\mu\eta\alpha^{5/3}+\tfrac{3}{2}\eta\alpha(1-\alpha)+\tfrac{3}{5}\eta(1-\alpha)^2. \tag{111}$$

In the limit $\mu\to+\infty$, the temperature of the transition behaves like

$$\eta_t\sim\frac{\ln\mu}{\mu}, \tag{112}$$

and the fraction of mass contained in the nucleus behaves like

$$1-\alpha\sim\frac{1}{\mu^2}. \tag{113}$$

The energy of the two phases at the transition point is given by

$$\Lambda_{gas}\sim-\frac{\mu}{\ln\mu},\quad \Lambda_{cond}-\Lambda_{max}(\mu)\sim-\frac{\mu}{\ln\mu}, \tag{114}$$

and the jump of the energy is

$$\Lambda_{cond}-\Lambda_{gas}\sim\mu. \tag{115}$$

For a given temperature, the thermodynamical parameters characterizing the condensate behave, in the limit $\mu\to+\infty$, like

$$1-\alpha_{cond}\sim e^{-\mu\eta},\quad \Lambda\sim\Lambda_{max}(\mu)\sim\mu,\quad J\sim\eta\Lambda_{max}(\mu)\sim\mu. \tag{116}$$

For the germ, we have

$$\alpha_{germ}\sim\left(\frac{\ln\mu}{\mu}\right)^{3/2},\quad \Lambda\to\Lambda_{gas},\quad J\to J_{gas}. \tag{117}$$

D. Comparision with previous works

Phase transitions in self-gravitating systems were first investigated with the aid of toy models that could be solved exactly without recourse to a mean-field approximation. For example, Lynden-Bell and Lynden-Bell [13] considered a system of N particles confined to the surface of a sphere of variable radius. They calculated exactly the density of states in the microcanonical ensemble and showed the existence of a region with negative specific heats. Then, they evaluated the partition function in the canonical ensemble and demonstrated that the region of negative specific heats is replaced by a remarkable giant phase transition connecting a ''gaseous'' phase (at high energies) to a ''condensed'' phase (at

low energies). Padmanabhan [1] obtained similar results with a simpler model consisting of only two particles in gravitational interaction confined within a spherical box. The phase diagram determined by these authors is similar to the one reported in Fig. 10. These models exhibit a phase transition in the canonical ensemble but not in the microcanonical ensemble (unlike in Fig. 7). This is because, for these simple models, the density of states remains finite when the small-scale cutoff a is set equal to zero, whereas for more realistic self-gravitating systems, it diverges. By contrast, the partition function is divergent for $a=0$ and this leads to the occurrence of a phase transition in the canonical ensemble when a is sufficiently small. Padmanabhan investigated the dependance of the critical parameters on the small-scale cutoff a. In particular, he found that the temperature of the transition is given by

$$T_t=\frac{Gm^2}{3a\ln(R/a)}. \tag{118}$$

This expression qualitatively agrees with our result (112), which becomes in dimensional variables

$$T_t\sim\frac{GN^{2/3}m^2}{a\ln(R/aN^{1/3})}. \tag{119}$$

Recall that $N=2$ in Padmanabhan's model. He also computed the change of the energy at the transition point and found that

$$E_{gas}-E_{cond}=\frac{Gm^2}{a}\left(1-\frac{1}{3\ln(R/a)}\right). \tag{120}$$

This expression also qualitatively agrees with our result (115), leading to

$$E_{gas}-E_{cond}\sim\frac{GN^{5/3}m^2}{a}. \tag{121}$$

The logarithmic correction in Eq. (120) is a particularity of Padmanabhan's model arising from the low value of N. Finally, Padmanabhan investigated the dependance of the $T(E)$ curve with the small-scale cutoff a (see his Fig. 3.2). For large a, his diagram is similar to that of Fig. 11. In particular, there exists a critical short distance cutoff above which the phase transition disappears (tricritical point). It should be stressed that the statistical approach based on the evaluation of $g(E)$ or $Z(\beta)$ does not determine the metastable states unlike the thermodynamical approach based on the maximization of $S[\rho]$ or $J[\rho]$. Only the true equilibrium states, which correspond to global maxima of S or J, appear in the $T(E)$ diagram (in other words, the ''plateaux'' are directly obtained without being required to make a Maxwell construction). These equilibrium states are expected to be reached for $t\to+\infty$ but they are not necessarily the most relevant for astrophysical applications: as discussed previously, the metastable equilibrium states may be long-lived and may correspond to the structures that are actually observed in the universe. Indeed, the statistical mechanical approach tells nothing about the time scales involved in the establishement of the equilibrium. A kinetic theory is needed to settle that point.

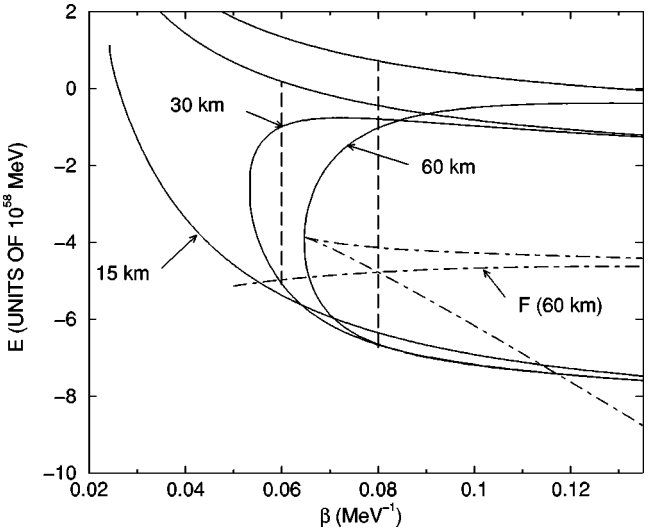

FIG. 23. Equilibrium phase diagram for a hard-sphere gas obtained in the framework of our analytical model. The parameters have been chosen so as to correspond to Fig. 2 of Aronson and Hansen [8]: $R=60$ km, $R=30$ km, $R=15$ km; $N=10^{57}$; $m=$ neutron mass$=1.67\times10^{-24}$ g; $a=0.4\times10^{-13}$ cm. These parameters correspond to a neutron-star-like structure. In our analytical model, we have adopted a value of the geometrical factor $g=2$ [8]. The agreement with the numerical study of Aronson and Hansen is fairly good. For small radius $R=15$ km, there is no phase transition. For larger radii ($R=30$ km, $R=60$ km), a phase transition connects the ''gaseous'' phase (upper branch) to the ''condensed'' phase (lower branch). This phase transition forms a Maxwell plateau (dashed line) at a temperature depending on the size R of the system [according to Eqs. (111) and (98)]. Dot-dashed lines represent the free energy $F=E-TS$ as a function of the inverse temperature for the case $R=60$ km. The crossing point determines the temperature of the transition.

Phase transitions in self-gravitating systems have also been investigated in the mean-field approximation for less idealized models. Aronson and Hansen [8] have considered the case of a classical hard-sphere gas modeled by a van der Waals equation of state. They considered a relatively large cutoff and evidenced only the phase transition in the canonical ensemble (they obtained a diagram similar to that of Fig. 10). They also proposed a simple analytical model to describe this phase transition. In their model, the ''gaseous'' phase consists of N particles spread with uniform density throughout the whole container and the ''condensed'' phase has *all* N particles collapsed into a central core of uniform density. The model that we proposed in Sec. VI is more general because we allow the condensate to contain an arbitrary fraction of the total mass. Then, the fraction of mass that is actually achieved at equilibrium is *determined* by maximizing the free energy vs α. In the canonical ensemble (the only situation discussed by Aronson and Hansen), the fraction of mass contained in the condensate is close to 1, so that our precedure provides additional support to their ansatz. However, our model allows us to describe also the unstable

solution with the ''germ'' ($\alpha \ll 1$) and to obtain a better representation of the whole bifurcation diagram (see Fig. 23). In addition, our model can also describe the phase transitions in the microcanonical ensemble (occuring for sufficiently small values of the cutoff a), which was not considered by Aronson and Hansen.

The study of Aronson and Hansen was reconsidered by Stahl *et al.* [9] who pointed out that the van der Waals equation of state does not adequately describe hard-sphere systems at high densities. They considered a more general equation of state and studied in detail the case of small filling factors for which a phase transition occurs in the microcanonical ensemble. They also determined numerically the dependance of the transition temperature (in the canonical ensemble) as a function of the filling factor and considered applications of their results in the context of planet formation.

Following the works of Aronson and Hansen [8] and Stahl *et al.* [9], different authors have attempted to describe phase transitions in self-gravitating systems by introducing a small-scale regularization of the gravitational potential. For example, in the study of Follana and Laliena [10], the softening is achieved by truncating to N terms an expansion of the Newtonian potential in spherical Bessel functions. These authors obtained an equilibrium phase diagram similar to the one in Fig. 10. However, they could not achieve very large values of N in their study so that they were not able to see the development of the spiral (and the corresponding phase transition in the microcanonical ensemble) as $N \to +\infty$. Another analysis of phase transitions in self-gravitating systems was provided by Youngkins and Miller [11] with a one-dimensional model of concentric spherical mass shells. They studied this system in the microcanonical, canonical, and grand canonical ensembles, both numerically and analytically, in the mean-field approximation. They found an overall good agreement between their numerical simulations and the mean-field predictions. They observed phase transitions in the microcanonical and canonical ensembles but not in the grand canonical ensemble in which the system remains homogeneous. This last result may be, however, an artifact of their one-dimensional model. It is plausible that, in the grand canonical ensemble, the self-gravitating gas fragments in a series of clumps (at different scales), as observed in cosmology and for the interstellar medium. Some theoretical arguments in favor of this scenario have been given by Semelin *et al.* [30] and Chavanis [25]. Of course, to study the development of these clumps, it is necessary to extend the thermodynamical analysis to the full three-dimensional problem and relax the assumption of spherical symmetry.

The thermodynamics of self-gravitating fermions was investigated by Lynden-Bell and Wood and Hertel and Thirring in the early 1970s (see the discussion of Aronson and Hansen [8]), but these papers were apparently not published. In Refs. [4,7], it is proved that a rigorous thermodynamic limit exists for self-gravitating fermions but the corresponding phase diagram is not explicitly given. This equilibrium phase diagram was calculated by Bilic and Viollier [5] for a particular value of the degeneracy parameter adapted to a cosmological settling. It was also calculated independantly by Chavanis and Sommeria [6] for an arbitrary degree of degeneracy in the context of the theory of ''violent relaxation.'' In Ref. [6], the development of the spiral for high values of the degeneracy parameter and the associated phase transition that occurs in the microcanonical ensemble (in addition to the more well-known phase transition in the canonical ensemble) was clearly shown. However, the point of the transition was not explicitly determined and this has been done in the present study.

E. Astrophysical applications

The application of the hard-sphere model in astrophysics could concern the fragmentation of the interstellar medium and the formation of stars or even smaller objects, such as planets [9]. These objects would correspond to the ''condensate'' that results from the collapse of a cloud of gas or dust. On the other hand, the model of self-gravitating fermions could have applications for massive neutrinos in dark matter models [16,5], white dwarfs [14], and neutron stars [15,4]. By cooling below a critical temperature, a condensed phase emerges consisting of a completely degenerate nucleus surrounded by a dilute envelope, as extensively studied in early models of stellar structure [14]. This model could also be relevant for the ''violent relaxation'' of collisionless stellar systems,[1] such as elliptical galaxies [17,6,20]. In that case, the exclusion principle is a consequence of the Liouville theorem. Since degeneracy can stabilize the system without changing its overall structure at large distances, we have suggested in Ref. [6] that degeneracy could play a role in galactic nuclei. The recent simulations of Leeuwin and Athanassoula [32] and the theoretical model of Stiavelli [33] are consistent with this idea especially if the nucleus of elliptical galaxies contains a primordial massive black hole. Indeed, the effect of degeneracy (in the sense of Lynden-Bell) on the distribution of stars surrounding the black hole can explain the cusps observed at the center of galaxies. Whether or not elliptical galaxies are degenerate remains however a matter of debate because when the core becomes dense, two-body encounters will come into play and break the Liouville theorem (Shu's criticism [34]). This form of degeneracy may, however, be relevant for massive neutrinos in dark matter models where it competes with quantum degeneracy [19]. In fact, the thermal equilibrium distribution of massive neutrinos in dark matter models might be justified more by the process of ''violent relaxation'' than by a collisional relaxation. Indeed, the time scale of gravitational two-body encounters for neutrinos is extremely long so that the criticism raised by Shu does not apply [35,19]. Therefore, the commonly adopted Fermi-Dirac distribution of self-gravitating neutrinos might be due to Lynden-Bell's type of degeneracy rather than due to quantum mechanics. Anyway, whatever the source of the exclusion principle (Lynden-Bell or Pauli),

[1]In fact, the problem is complicated because violent relaxation eventually fades before the maximum entropy state is attained. Thus, Eq. (6) [or Eq. (7)] is unlikely to be reached throughout the whole cluster. However, it is reasonable to hold in the central region in which violent relaxation occurs most violently [17,31].

the self-gravitating Fermi-Dirac model predicts the formation of a dense degenerate nucleus (fermion ball) with a small radius and a large mass [5,6]. As suggested in Refs. [5,36], this dense degenerate nucleus could be an alternative to black holes at the center of galaxies. On the other hand, at large distances, the density of the self-gravitating Fermi gas decays like r^{-2}, which is a condition that dark galactic halos must fulfill in order to reproduce the flat rotation curves of spiral galaxies [22]. Therefore, this model of self-gravitating fermions has a chance to account for the structure of dark matter in galactic halos.

VII. CONCLUSION

In this paper, we have described the inequivalence of statistical ensembles and the nature of phase transitions in self-gravitating systems by considering the case of self-gravitating fermions or the case of a classical hard-sphere gas. The introduction of an effective repulsion at short distances avoids the singularity of the ''naked'' gravitational potential. It is likely that similar results will be obtained with different forms of regularization. For large values of the cutoff a, there are no phase transitions. For intermediate values of a, phase transitions occur in the canonical ensemble but not in the microcanonical ensemble. The corresponding phase diagram is of the type of Fig. 10 and has been found by various authors [8,5,6,10]. For smaller values of a, phase transitions occur both in the canonical and in the microcanonical ensemble. The corresponding phase diagram is of the type in Fig. 7 and was first obtained in Ref. [6]. As the small-scale cutoff is decreased, the $T(E)$ curve winds up and tends to the classical spiral for $a\rightarrow 0$ (see Fig. 1).

Depending on the value of the cutoff a and of the ensemble considered (microcanonical or canonical), three kinds of phase transitions can be evidenced, which separate a ''gaseous'' phase from a ''condensed'' phase. In the microcanonical ensemble and for sufficiently small a (Fig. 7), a gravitational first order phase transition occurs at an energy $E_t(a)$ at which the ''gaseous'' states pass from global to local entropy maxima and the ''condensed'' states from local to global entropy maxima. This transition is marked by a discontinuity of the temperature and of the specific heats. In the limit $a\rightarrow 0$, the transition energy is rejected to $+\infty$, so that the stable (gaseous) solutions of the classical spiral are only *metastable*. These states may be physical, depending on whether the initial condition lies in their ''basin of attraction'' or not [6,11,26]. However, the metastable branch disappears at a critical energy E_c, discovered by Antonov [2], at which the ''gravothermal catastrophe'' [3] occurs. This collapse can be considered as a zeroth order phase transition since it is associated with a discontinuity of entropy. For larger values of a, there is only one entropy maximum for each value of energy (Fig. 10) and the previously described phase transitions are suppressed. However, as we progressively decrease the energy, the self-gravitating gas achieves higher and higher density contrasts and builds up a compact core containing more and more mass. This gravitational ''clustering'' can be called a second order phase transition since the specific heats diverges at the critical point η_c and the order parameter experiences a rapid variation in the region of negative specific heats (but remains continuous). Similar phase transitions occur in the canonical ensemble. It is interesting that these phase transitions can be understood with the aid of a simple analytical model that allows one to determine the dependance of the thermodynamical parameters with the cut-off value. The present study can be extended to include rotation [38]. It is also important to develop nonequilibrium models to determine the structure of the ''basin of attraction'' of the equilibrium states when several entropy maxima exist. A first step in that direction was made by Youngkins and Miller [11] and by Chavanis *et al.* [26] with the aid of simplified dynamical models. These models could be used, in particular, to investigate numerically the occurrence of the phase transitions and the robustness of the metastable states. If the system is placed in a metastable state (local entropy maximum), it will eventually jump to the global entropy maximum, but this can take an infinite (physically irrelevant) time. Indeed, the probability that a fluctuation will allow the phase transition to develop is expected to be extremely low (except near the critical point Λ_c) [37]. Therefore, if the system is trapped in a metastable state (but still slowly evolving along the series of equilibrium by losing mass or energy, such as for globular clusters), the phase transition will occur at the critical point Λ_c rather than at Λ_t. However, if the system is initially far from equilibrium, there is no simple criterion to decide *a priori* whether it will converge towards the local or the global entropy maximum. Only direct numerical simulations can answer this question and sketch the structure of the basin of attraction for self-gravitating systems.

ACKNOWLEDGMENTS

I acknowledge interesting discussions with N. Bilic, T. Dauxois, O. Fliegans, V. Laliena, D. Lynden-Bell, C. Sire, and J. Sommeria. Special thanks are due to J. Katz for useful comments on the manuscript. I have also benefitted from valuable discussions with S. Ruffo, J. Barré, and F. Bouchet during my stay at the University of Firenze.

APPENDIX: ENTROPY OF THE SELF-GRAVITATING FERMI GAS

In this Appendix, we give the main steps for deriving the expression (17) for the entropy. Substituting the Fermi-Dirac distribution

$$f=\frac{\eta_0}{1+ke^{\psi}e^{\beta v^2/2}}, \tag{A1}$$

in the entropy (5) we obtain after some rearrangements

$$\eta_0 S = M\ln k+\int \rho\psi d^3\mathbf{r}+K\beta + \eta_0\int \ln\left(1+\frac{1}{k}e^{-\psi}e^{-\beta v^2/2}\right)d^3\mathbf{r}d^3\mathbf{v}. \tag{A2}$$

The last integral can be integrated by parts yielding the value $2\beta K/3$. Therefore,

$$\eta_0 S = M \ln k + \int \rho \psi d^3\mathbf{r} + \frac{5}{3} K\beta. \tag{A3}$$

Using the definition of ψ, we get

$$\eta_0 S = M \ln k + 2\beta W - M\beta\Phi_0 + \tfrac{5}{3} K\beta. \tag{A4}$$

Now, the central density is determined by the relation $\psi(\alpha) = \beta(\Phi(R) - \Phi_0)$ with $\Phi(R) = -GM/R$. Hence

$$\frac{S\eta_0}{M} = \ln k + \frac{2\beta}{M} W + \frac{\beta GM}{R} + \psi(\alpha) + \frac{5\beta K}{3M}. \tag{A5}$$

Using Eq. (3.12) of Chavanis and Sommeria [6] to express the potential energy W and the kinetic energy $K = E - W$ in terms of E, we find

$$\frac{S\eta_0}{M} = \ln k + \eta + \psi(\alpha) - \frac{7}{3}\Lambda\,\eta - \frac{2}{9}\,\eta\,\frac{\alpha^{10}}{\mu^4} I_{3/2}(k e^{\psi(\alpha)}). \tag{A6}$$

Finally, using $\eta = \mu^2/\alpha^4$, resulting from Eqs. (13) and (15), we obtain Eq. (17).

[1] T. Padmanabhan, Phys. Rep. **188**, 285 (1990).
[2] V. A. Antonov, Vest. Leningr. Gos. Univ. **7**, 135 (1962).
[3] D. Lynden-Bell and R. Wood, Mon. Not. R. Astron. Soc. **138**, 495 (1968).
[4] P. Hertel and W. Thirring, Commun. Math. Phys. **24**, 22 (1971).
[5] N. Bilic and R. D. Viollier, Phys. Lett. B **408**, 75 (1997).
[6] P. H. Chavanis and J. Sommeria, Mon. Not. R. Astron. Soc. **296**, 569 (1998).
[7] R. Robert, Class. Quantum Grav. **15**, 3827 (1990).
[8] E. B. Aronson and C. J. Hansen, Astrophys. J. **177**, 145 (1972).
[9] B. Stahl, M. K. H. Kiessling, and K. Schindler, Planet. Space Sci. **43**, 271 (1994).
[10] E. Follana and V. Laliena, Phys. Rev. E **61**, 6270 (2000).
[11] V. P. Youngkins and B. N. Miller, Phys. Rev. E **62**, 4582 (2000).
[12] J. Barré, D. Mukamel, and S. Ruffo, Phys. Rev. Lett. **87**, 030601 (2001).
[13] D. Lynden-Bell and R. M. Lynden-Bell, Mon. Not. R. Astron. Soc. **181**, 405 (1997).
[14] S. Chandrasekhar, *An Introduction to the Theory of Stellar Structure* (Dover, New York, 1942).
[15] J. R. Oppenheimer and G. M. Volkoff, Phys. Rev. **55**, 374 (1939).
[16] G. Ingrosso, M. Merafina, R. Ruffini, and F. Strafella, Astron. Astrophys. **258**, 223 (1992).
[17] D. Lynden-Bell, Mon. Not. R. Astron. Soc. **136**, 101 (1967).
[18] P. H. Chavanis, J. Sommeria, and R. Robert, Astrophys. J. **471**, 385 (1996).
[19] A. Kull, R. A. Treumann, and H. Böringer, Astrophys. J. Lett. **466**, L1 (1996).
[20] P. H. Chavanis, in *Proceedings of the Conference on Multiscale Problems in Science and Technology*, edited by N. Antonic, C. J. van Duijn, W. Jäger, and A. Rikelic (Springer, Berlin, 2002).
[21] P. H. Chavanis, Mon. Not. R. Astron. Soc. **300**, 981 (1998).
[22] J. Binney and S. Tremaine, *Galactic Dynamics*, Princeton Series in Astrophysics (Princeton, New Jersey, 1987).
[23] J. Katz, Mon. Not. R. Astron. Soc. **183**, 765 (1978).
[24] T. Padmanabhan, Astrophys. J., Suppl. **71**, 651 (1989).
[25] P. H. Chavanis, Astron. Astrophys. **381**, 340 (2002).
[26] P. H. Chavanis, C. Rosier, and C. Sire, e-print cond-mat/0107345.
[27] P. H. Chavanis, Astron. Astrophys. **381**, 709 (2002).
[28] H. J. de Vega and N. Sanchez, Nucl. Phys. B **625**, 409 (2002).
[29] M. Cerruti-Sola, P. Cipriani, and M. Pettini, Mon. Not. R. Astron. Soc. **328**, 339 (2001).
[30] B. Semelin , H. J. de Vega, and N. Sanchez, Phys. Rev. D **59**, 125021 (1999).
[31] J. Hjorth and J. Madsen, Mon. Not. R. Astron. Soc. **253**, 703 (1991).
[32] F. Leeuwin and E. Athanassoula, Mon. Not. R. Astron. Soc. **417**, 79 (2000).
[33] M. Stiavelli, Astrophys. J. Lett. **495**, L91 (1998).
[34] F. H. Shu, Astrophys. J. **225**, 83 (1978).
[35] J. Madsen, Astrophys. J. **316**, 497 (1987).
[36] N. Bilic, R. J. Lindebaum, G. B. Tupper, and R. D. Viollier, Phys. Lett. B **515**, 105 (2001).
[37] J. Katz and I. Okamoto, Mon. Not. R. Astron. Soc. **317**, 163 (2000).